# Prediction of the response of selected geotechnical structures using advanced nonlinear constitutive models

A. Zemanová, M. Šejnoha, B. Polák and P. Ch. Do

August 21, 2025

**Affiliation**
Ing. Alena Zemanová, Ph.D., Czech Technical University in Prague, Faculty of Civil Engineering, Department of Geotechnics
Prof. Ing. Michal Šejnoha, Ph.D., DSc., Czech Technical University in Prague, Faculty of Civil Engineering, Department of Mechanics
Ing. Barnabás Polák, FINE ltd.
Phuong Chinh Do, MSc., Charles University, Faculty of Science, Institute of Hydrogeology, Engineering Geology and Applied Geophysics

## Contents

# 1 Motivation

It is doubtless the fact that the theoretical background of practitioners is overgrowing. Consequently, application of advanced constitutive models is no longer domain of university scientists but becomes common to even a relatively small engineering projects. Most companies now rely on several computational resources allowing in turn for the verification of a given theoretical design. Inquired generally by design engineers the GEO5 has recently implemented into its FEM software the Hardening soil and Soft soil models to support the currently available suite of advanced constitutive models. While adopting most simple models usually based on the premise of perfect plasticity does not typically yield significant deviations in the response prediction provided by two distinct softwares, application of complex constitutive models, which may differ in some implementation details, should be approached with caution. Self-evident are deviations caused by blindly accepting values of certain model parameters calibrated on the basis of a specific formulation pertinent to a given software in another software, in which the implementation may follow a slightly different theoretical grounds. It is therefore of paramount importance to became familiar with at least the principal differences in the formulation of such an advanced constitutive model when comparing predictions derived from two particular softwares.

The goal here is thus to discuss, through several illustrative examples, a number of phenomena which may arise as direct consequence of a specific formulation of a given constitutive model. To this end, we choose the Hardening soil model which has gained a considerable popularity among practical engineers. Because conceived within the research group with close link to Plaxis [3], we adopt this software as a source for the verification of this model implementation in the GEO5 FEM [2].

The present study examines two potential directions in the modeling of a certain engineering task while exploiting two different softwares:

1. Assume no knowledge about the model formulation and implementation in individual softwares and use the same set of data in both softwares. We mention in advance that this would correspond to employing the set of data stored in the first row in Table 2. Unfortunately, as mentioned later, some of the data are not directly available to Plaxis users. So such a direct comparison might not always be possible.

2. Accept potential differences in the model formulation and use the Plaxis data to first simulate a set of standard laboratory tests such as oedometer and drained triaxial tests. Next, adopt the generated data for example in ExCalibre software [1] to calibrate the model parameters associated with the formulation of the Hardening soil model used in GEO5 FEM. This would be the standard procedure to follow providing the real laboratory measurements are available.

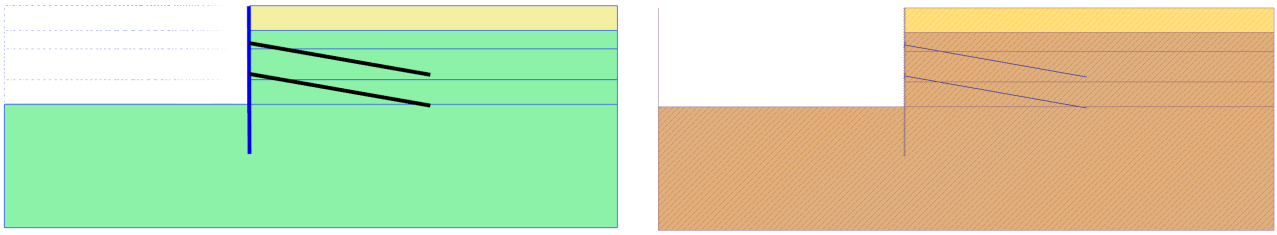

(a) (b)

Figure 1: Illustrative figure: a) Plaxis, b) GEO5 FEM

## 2 Introduction

Two illustrative examples are presented to compare predictions provided by Plaxis and GEO5 FEM softwares with particular attention to the application of Hardening soil model (HSM). It is the intention of this study to alert the reader to potential differences in the predicted response owing to several dissimilarities in the implementation of this highly complex constitutive model. For example, the yield surfaces in Plaxis are defined in the principal stress state while in GEO5 FEM the yield surfaces are defined in terms of equivalent stress and strain measures, see Fig. 2 and the formulations presented in corresponding theoretical manuals [2, 3].

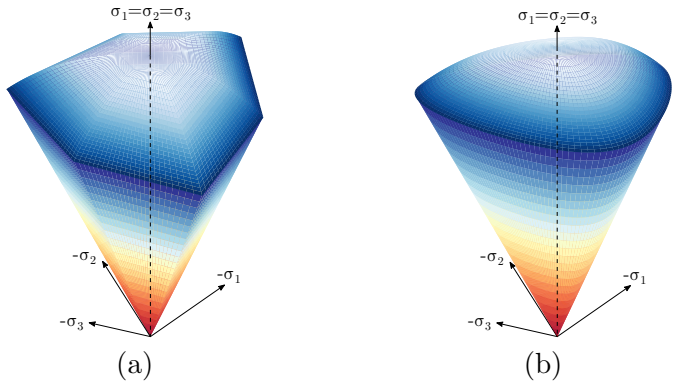


Figure 2: Yield surfaces in principal stress space: a) Plaxis, b) GEO5 FEM

However, it goes beyond the present scope to mention all the details concerning the two implementations. So just for illustration we mention yet another relatively important difference which is the formulation of the elastic stiffness written as

$$E_{ur} = E_{ur}^{\text{ref}} \left( \frac{\sigma_3 + c\cot\varphi}{p^{\text{ref}} + c\cot\varphi} \right)^{m}, \qquad \text{Plaxis,} \tag{1}$$

$$E_{ur} = E_{ur}^{p,\text{ref}} \left( \frac{\sigma_m + c\cot\varphi}{\sigma_m^{\text{ref}} + c\cot\varphi} \right)^{m_p}, \qquad \text{GEO5 FEM} \tag{2}$$

where $\sigma_3$ is the minor principal stress and $\sigma_m = \frac{1}{3}(\sigma_1 + \sigma_2 + \sigma_3)$ is the mean effective stress. While the Plaxis formulation enjoys the benefit of keeping the stiffness evolution independent of stress variation in triaxial compression, the GEO5 implementation avoids principal stress migration upon loading-unloading-reloading sequence. It is also perhaps evident that the driving stiffness parameters may differ when fitting the two models to the same experimental data. To see this, we open our discussion with the calibration of GEO5-HS model parameters based on the synthetic data generated by Plaxis. Simulation of foundation settlement and the behavior of an anchored retaining wall is examined next.

## 3 Calibration of GEO5-HS model parameters

The program ExCalibre allows us to calibrate the GEO5-HS model parameters based on the measurements acquired from the oedometer and triaxial tests. In the present study, such measurements were generated exploiting the Plaxis-SoilTest program for the selected Plaxis-HS model parameters listed in Table 1.

Table 1: Plaxis-HS model parameters $\varphi = 30°$, $\psi = 0$, $\nu_{ur} = 0.2$

| $E_{ur}^{\text{ref}}$ [kPa] | $E_{50}^{\text{ref}}$ [kPa] | $m$ [-] | $R_f$ [-] | $M$ [-] | $H$ [kPa] | $c$ [kPa] |
|---|---|---|---|---|---|---|
| 22500 | 7500 | 0.90 | 0.90 | 0.512 | 183241 | 5 |

Note that the peak angle of internal friction $\varphi = 30°$, the peak angle of dilation $\psi = 0$, and the Poisson ratio $\nu_{ur}$ were kept the same in both models. Also point out that the cap parameters $M$ and

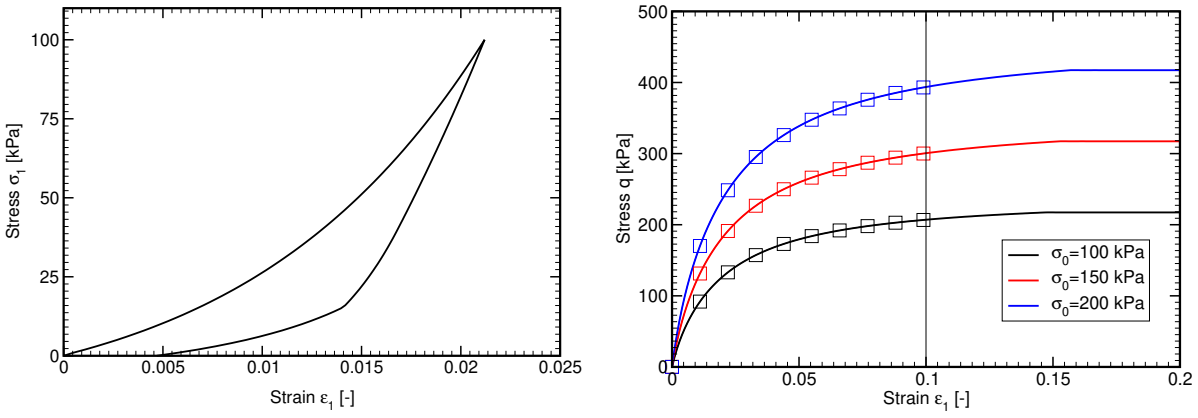


(a) (b)

Figure 3: Synthetic data generated by Plaxis-SoilTest for the set of model parameters in Table 1: a) oedometer, b) drained triaxial compression

$H$ were derived such as to match the coefficient of lateral earth pressure at rest $K_0^{NC} = 0.5$ and the oedometric modulus $E_{oed} = 9000$ kPa at the reference pressure $p^{ref} = 100$ kPa (reference oedometric stress $\sigma_{oed}^{ref} = 100$ kPa in GEO5 FEM).

In particular, the data from one oedometer test and three drained triaxial tests performed at chamber pressures $\sigma_0 = 100, 150, 200$ kPa were utilized in the calibration step. The corresponding plots are shown in Fig. 3.

Table 2: GEO5-HS model parameters $\varphi = 30°$, $\psi = 0$, $\nu_{ur} = 0.2$

| **soil** | $E_{ur}^{p,\text{ref}}$ [kPa] | $E_{50}^{p,\text{ref}}$ [kPa] | $m_p$ [-] | $R_f$ [-] | $M$ [-] | $H$ [kPa] | $c$ [kPa] | Note |
|---|---|---|---|---|---|---|---|---|
| 1 | 22500 | 7500 | 0.90 | 0.90 | 0.512 | 183241 | 5 | Plaxis data, see Table 1 |
| 2 | 18000 | 7500 | 0.87 | 0.90 | 0.512 | 183241 | 5 | $E_{ur}^{p,\text{ref}}, m_p$ modified, $M, H$ from Plaxis |
| **3** | 22500 | 7500 | 0.90 | 0.90 | 1.024 | 32846 | 5 | $M, H$ from GEO5 |
| **4** | 18000 | 7500 | 0.87 | 0.90 | 0.890 | 25847 | 5 | $E_{ur}^{p,\text{ref}}, m_p$ modified, $M, H$ from GEO5 |
| **5.1** | 19070 | 9192 | 0.80 | 0.99 | 0.750 | 54550 | 5.2 | triaxial up to $\varepsilon_1 = 0.1$ |
| **5.2** | 19070 | 8145 | 0.64 | 0.90 | 0.740 | 54466 | 4.2 | triaxial up to $\varepsilon_1 = 0.2$ |

The results of the calibration step appear in the last two rows of Table 2. These are identified as soils No. **5.1** and **5.2**, respectively. The difference between the two sets of parameters is the maximum major principal strain $\varepsilon_1$ to generate the synthetic data. Recall that the deviatoric stress measure $q$ in Fig. 3(b) is defined for the drain triaxial compression as

$$q = \sigma_1 - \sigma_3. \tag{3}$$

Apart from the calibrated model parameters, another two sets of model parameters labeled as soils No. **3** and **4** were considered in simulations. The soil No. **3** assumes the basic material data identical to those used in Plaxis with the cap parameters derived using the GEO5 FEM software. The soil No. **4** considers the adjusted stiffness parameters $E_{ur}^{p,\text{ref}}$ and $m_p$ found such as to match the nonlinear elastic response in oedometer as described in the theoretical manual [2].

To compare the predictions provided by GEO5 FEM with the synthetic data generated by Plaxis we start from the results attributed to soils No. **3** and **4** displayed in Fig. 4. Note that the solid black line was constructed with GEO5 FEM using the same data as used in Plaxis including the cap parameters (soil No. 1 in Table 2). The solid orange line corresponds to model parameters of soil No. **2** (with reduced stiffness $E_{ur}^{p,\text{ref}}$ and adopting the Plaxis cap parameters from Table 1). However, these parameters are generally hidden to Plaxis users. It is interesting to point out that with this set of data almost a perfect match in oedometer test can be achieved. On the contrary, the largest mismatch is observed for the drained triaxial compression for the same set of data. It thus appears

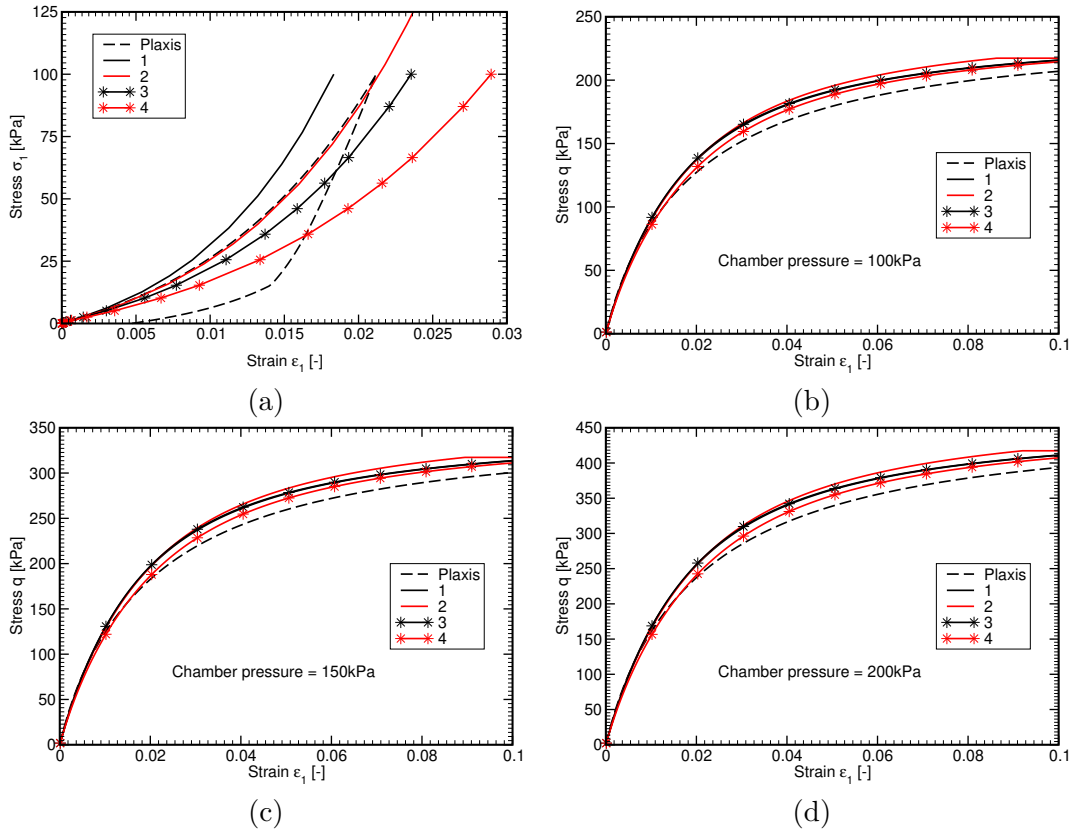


Figure 4: Oedometer (OED) and drained triaxial compression (TRIAX) tests. Comparing predictions provided by GEO5 FEM for soils No. 1-4 with synthetic data generated by Plaxis-SoilTest: a) OED, b) TRIAX, chamber pressure $\sigma_0 = 100$ kPa, c) TRIAX, $\sigma_0 = 150$ kPa, d) TRIAX, $\sigma_0 = 200$ kPa

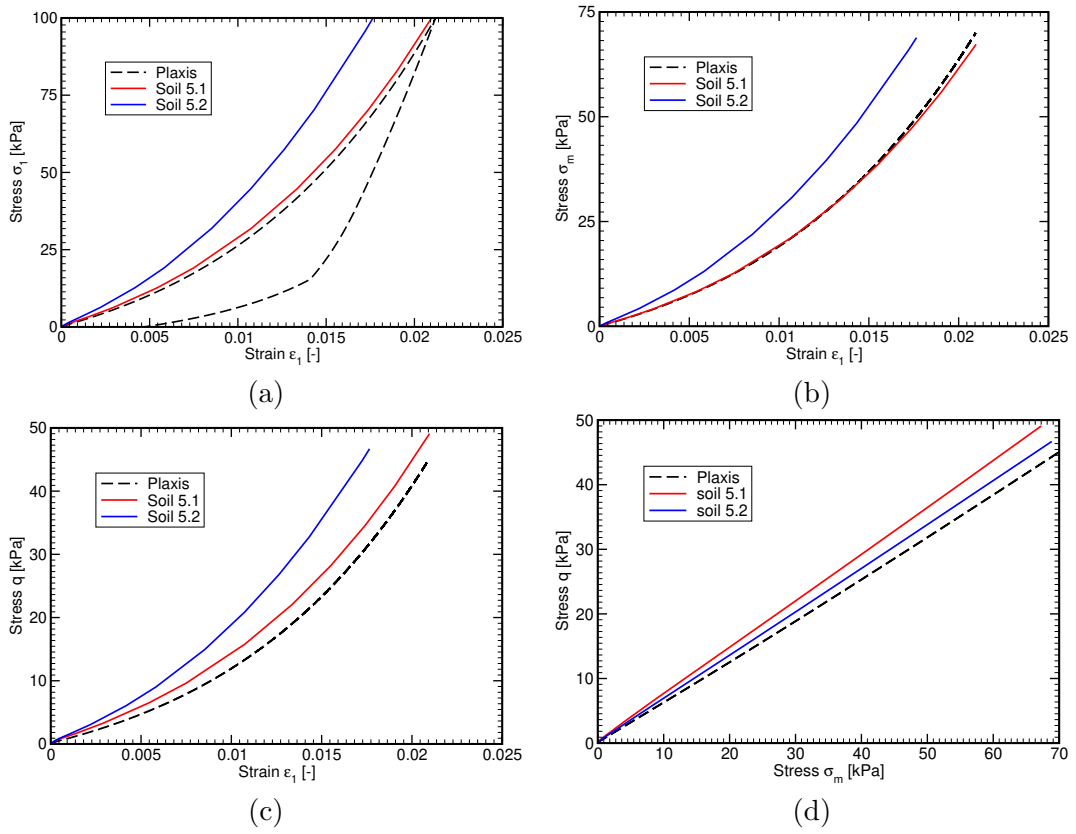


Figure 5: Results of calibration step, soils No. **5.1** and **5.2** - oedometer test: a) $\varepsilon_1 - \sigma_1$ diagram, b) $\varepsilon_1 - \sigma_m$ diagram, c) $\varepsilon_1 - q$ diagram, d) $\sigma_m - q$ diagram

rather challenging to obtain a unique set of GEO5-HS model parameters which allows for matching both oedometer and triaxial tests sufficiently accurately. When adopting purely Plaxis-HS data the oedometric response provided by GEO5 FEM is generally stiffer in comparison to Plaxis predictions.

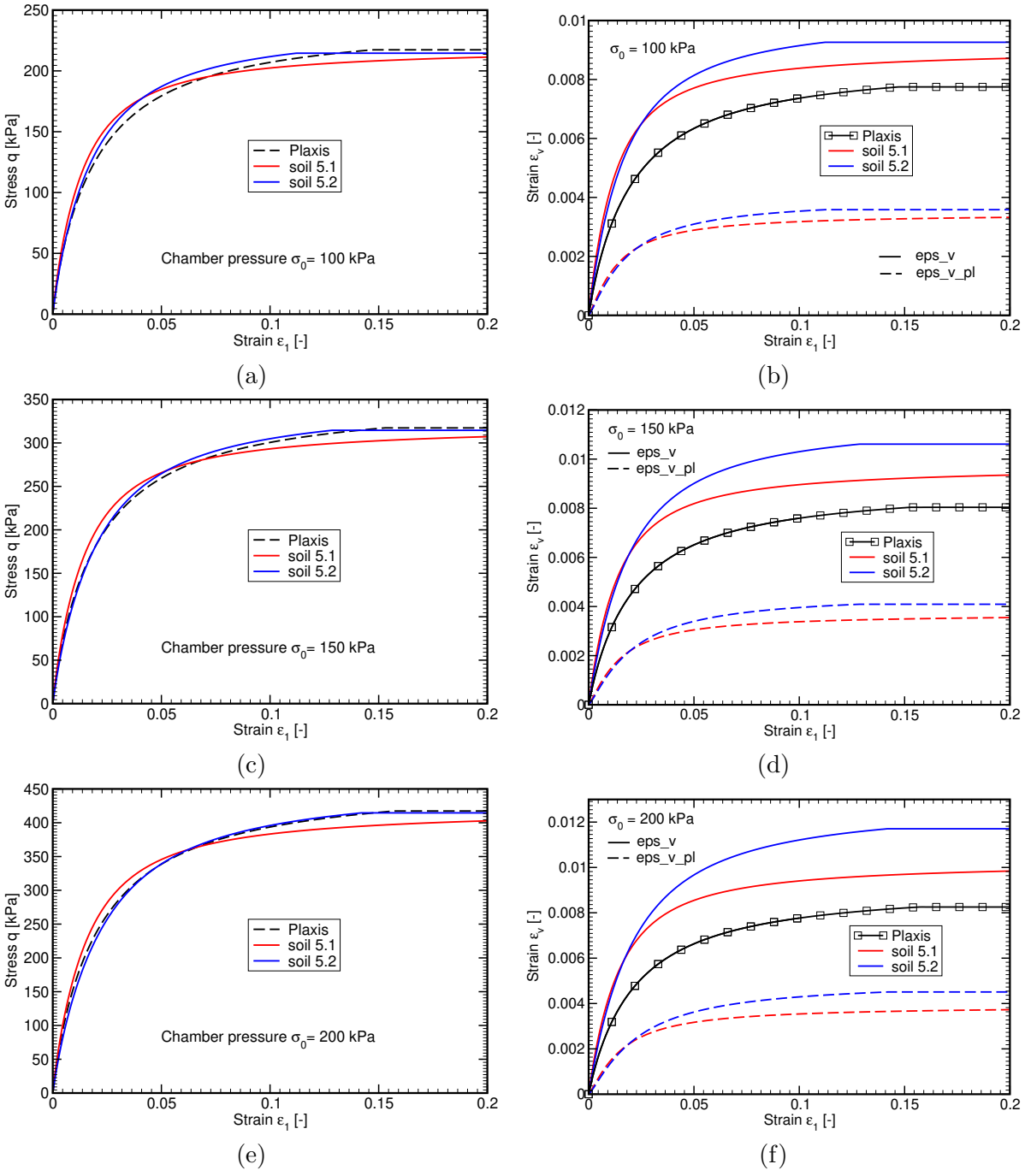


Figure 6: Results of calibration step, soils No. **5.1** and **5.2** - drain triaxial compression test - (a,b) $\sigma_0 = 100$ kPa, (c,d) $\sigma_0 = 150$ kPa, (e,f) $\sigma_0 = 200$ kPa: a) $\varepsilon_1 - q$ diagram, b) $\varepsilon_1 - \sigma_v$ diagram, c) $\varepsilon_1 - q$ diagram, d) $\varepsilon_1 - \sigma_v$ diagram, e) $\varepsilon_1 - q$ diagram, f) $\varepsilon_1 - \sigma_v$ diagram

The results of the calibration step are demonstrated in Figs. 5 - 7. First, the synthetic data generated by Plaxis from drained triaxial compression tests were terminated at the maximum strain $\varepsilon_1 = 10\%$ (the part of curves labeled with square symbols in Fig. 3(b)). Adopting these curves in the calibration step resulted in GEO5-HS model parameters denoted as soil No. **5.1** in Table 2. When exploiting the curves in Fig. 3(b) for the entire range of strain up to $\varepsilon_1 = 20\%$ we arrived at a set of model parameters labeled as soil No. **5.2** in Table 2.

A graphical representation of the oedometric curve in Fig. 5(a) suggests a much stiffer response of

soil No. **5.2** when compared to the prediction derived for soil No. **5.1**. This also applies to invariant stress measures $\sigma_m$ (the mean effective stress) and $q$ (the deviatoric stress).

On the other hand, the model parameters attributed to soil No. **5.2** provide a better fit to triaxial tests as seen in Figs. 6(a,c,e). Nevertheless, the bulk response, unlike the response in a uniaxial compression, seems more compliant for both sets of data resulting into a notable deviation of GEO5 FEM predictions from the Plaxis data, see Figs. 6(b,d,f) where $\varepsilon_v = \varepsilon_1 + 2\varepsilon_3$ is the total volumetric strain. The evolution of plastic volumetric strain is also shown for illustration. It is evident that the volumetric plastic strain is essentially negligible. This is supported by the stress-strain diagrams in Fig. 7 suggesting more or less linear variation of the mean stress as a function of the volumetric strain. Note that the slopes of these diagrams identify the bulk modulus of a given soil. The already mentioned more compliant response predicted by GEO5 FEM in comparison to Plaxis is also evident.

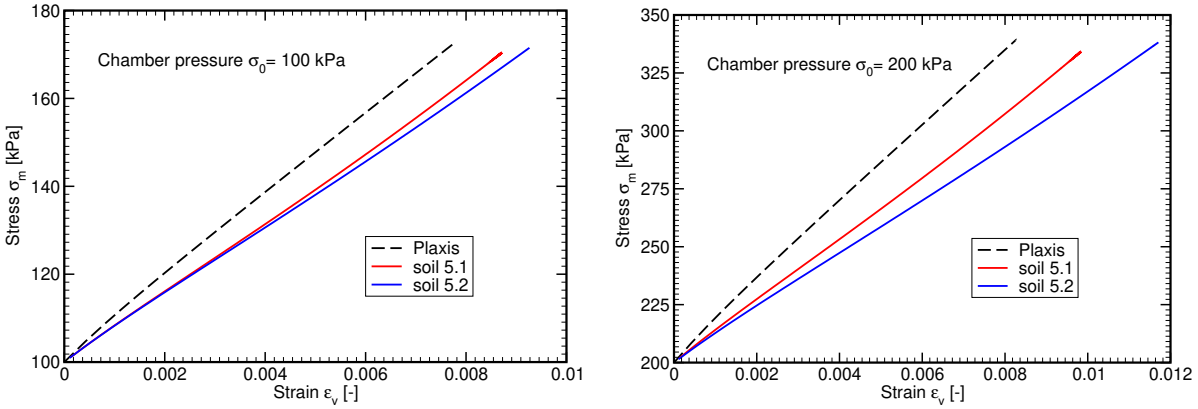


(a) (b)

Figure 7: Bulk response - stress strain diagrams: a) chamber pressure $\sigma_0 = 100$ kPa, a) chamber pressure $\sigma_0 = 200$ kPa

The above results allow for the following partial conclusion:

- **Although evident from visual inspection, the generated differences attributed to individual sets of data appear insignificant at least from the engineering point of view**.
- A minor impact on the estimated response of a real engineering task might therefore be expected.

Addressing these issues thus becomes our next objective. Herein, attention is limited to the prediction of settlement of a strip footing and the behavior of a sheeting wall at various stages of excavation. In both examples, the analysis was first performed with the Mohr-Coulomb model in order to tune the computational model. The model parameters of the Mohr-Coulomb model are available in Table 3.

Table 3: Tested MC model parameters

| | | | |
|---|---|---|---|
| Unit weight | $\gamma =$ | 20 | kN $\cdot$ m $^{-3}$ |
| Young's modulus | $E = E_{ur} =$ | 20 | MPa |
| Poisson's ratio | $\nu =$ | 0.2 | [-] |
| Friction angle | $\varphi =$ | 25 | $^\circ$ |
| Cohesion | $c =$ | 15 | kPa |
| Dilatancy angle | $\psi =$ | 0 | $^\circ$ |
| Coefficient of earth pressure at rest | $K_0^{NC} =$ | 0.5 | [-] |

# 4 Strip footing settlement

The first example is concerned with the prediction of settlement of a strip footing. The computational model is assumed to be 7m wide and 3m deep. Finite element meshes composed of 6-noded triangular elements in both Plaxis and GEO5 FEM softwares are plotted in Fig. 8. The blue line in Fig. 8(a) indicates the position of footing which is represented here by a sufficiently stiff beam element (height of beam $h = 1$m, concrete type C20/25). No interface elements are considered in this study.

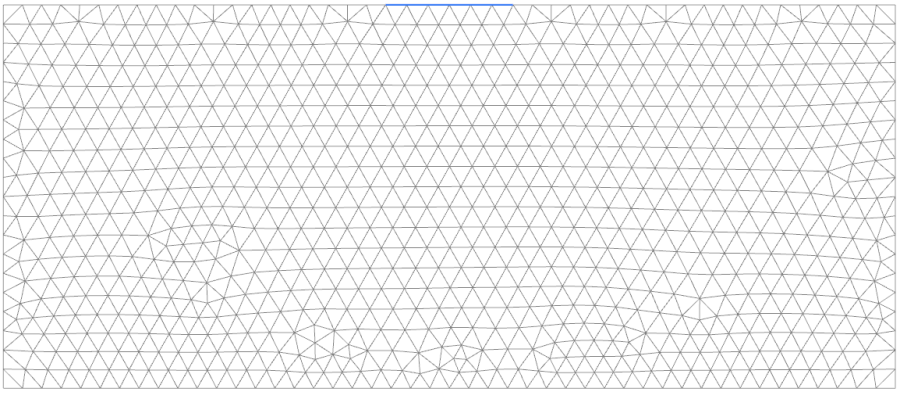

(a)

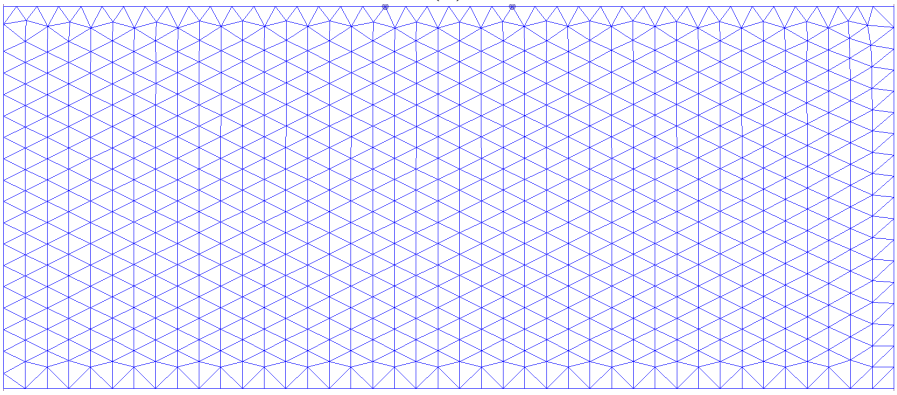

(b)

Figure 8: 6-noded triangular elements with edge size of about 0.17 m: a) Plaxis, b) GEO5 FEM

The actual analysis was carried out in five calculation stages:

1. The $K_0$ procedure was used to generate the initial stress state. This stage also served to initialize the state variables of HSM, i.e., the preconsolidation pressure $p_c$ (denoted as $p_p$ in Plaxis) and the shear hardening parameters $\gamma_p$ and $\kappa_s$ used in Plaxis and GEO5 FEM, respectively. These parameters are set such that the stress state in every material point satisfies both the shear and cap yield criteria. It is perhaps useful to remind the definition of shear hardening parameters written as
$$\kappa_s = \sum \sqrt{2\Delta e_{ij}^{pl} \Delta e_{ij}^{pl}}, \qquad \gamma_p = \frac{\sqrt{3}}{2}\kappa_s \tag{4}$$
where $\Delta e_{ij}^{pl}$ represents components of the increment of deviatoric plastic strain tensor. Point out that the evolution of preconsolidation pressure also differs in both implementations.

2. An overburden pressure of 20 kPa, corresponding to 1m deep layer of soil, was applied next over the entire surface to avoid potential issues which may arise with soil elements of very low stiffness close to the terrain surface.

3. The soil in the region of strip footing was then unloaded to zero vertical stress.

4. The stiff strip footing was installed introducing additional load due to self-weight.

5. Finally, the strip footing was gradually loaded by a uniform pressure up to the value of 200 kPa.

### 4.1 Simulations with Mohr-Coulomb model

Applicability of the proposed computational model was first checked by comparing the predicted settlement for the Mohr-Coulomb. The resulting vertical displacement at the center of strip footing at the end of individual calculation stages is stored in Table 4. It is evident that both softwares deliver the same response for this simple elastic perfectly plastic model, see also the plots of vertical displacements along the strip footing, the surface plots of vertical displacements, and the distribution of bending moment along the beam axis in Fig. 9.

These results thus support the expectation suggested already in the first paragraph in Section 1 with reference to simple computational model as well as promote application of both computational models to run a comparative study with the complex Hardening soil model.

Table 4: Settlement at the center of strip footing [mm]

| Calculation stage | Plaxis | GEO5 FEM |
|---|---|---|
| 1. Initial stresses | 0 | 0 |
| 2. Surface surcharge of 20 kPa | 2.7 | 2.7 |
| 3. Unloading | 1.3 | 1.3 |
| 4. Strip footing self-weight | 2.8 | 2.8 |
| 5. Uniform pressure of 200 kPa | 25.8 | 25.7 |

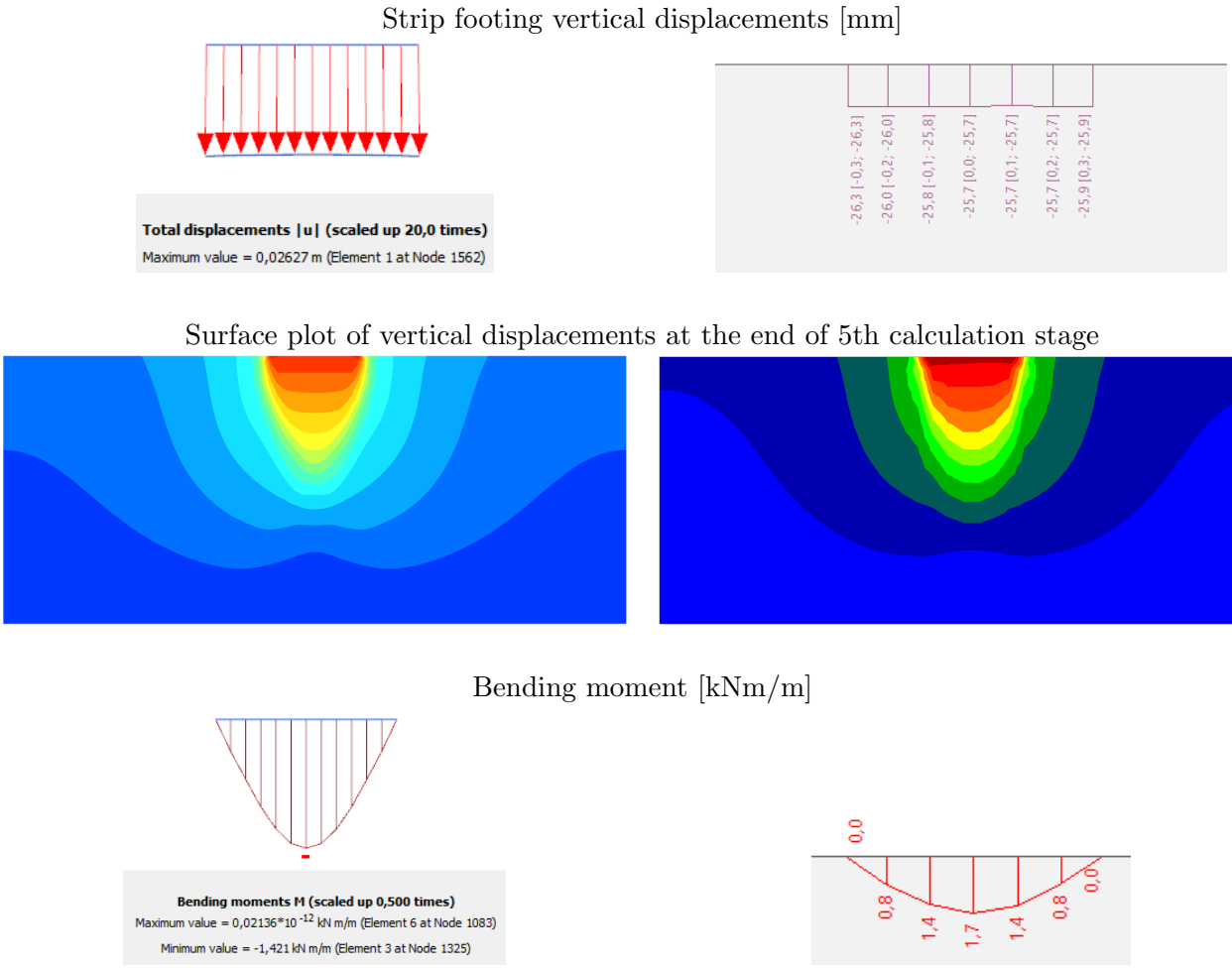


Figure 9: Comparison of selected results generated by Plaxis (left) and GEO5 FEM (right) outputs for the final calculation stage

### 4.2 Simulation with Hardening soil model

As already demonstrated in Eq. (4) various softwares might use different equivalent stress or strain measures. With reference to the presented results it thus appears useful to recall definitions of the equivalent deviatoric strain measures used in Plaxis and GEO5 FEM. In Plaxis the equivalent deviatoric strain measure $\varepsilon_q$ is provided by

$$\varepsilon_q = \sqrt{\frac{2}{3} e_{ij} e_{ij}} \tag{5}$$

whereas in GEO5 FEM the equivalent deviatoric strain $E_d$ is given by

$$E_d = \sqrt{2 e_{ij} e_{ij}} \quad \text{so that} \quad \varepsilon_q = \frac{1}{\sqrt{3}} E_d \tag{6}$$

where $e_{ij}$ stands for the components of the deviatoric strain tensor.

As already mentioned, the $K_0$-procedure serves to generate the initial values of hardening parameters. Their evolution begins with the 2nd calculations stage. The distribution of their initial values is graphically presented in Fig. 10 showing also their extreme values. Note that the colors might not match isosurfaces generated by Plaxis and GEO5 FEM softwares. It is already seen that different implementation of both shear and cap yield surfaces, together with different values of model parameters, i.e., the cap parameter $M$, may lead to different initial values already prior to any additional loading. Remind that the yield surfaces in Plaxis are defined in the principal stress state while in GEO5 FEM the yield surfaces are defined in terms of equivalent stress and strain measures, recall Fig. 2.

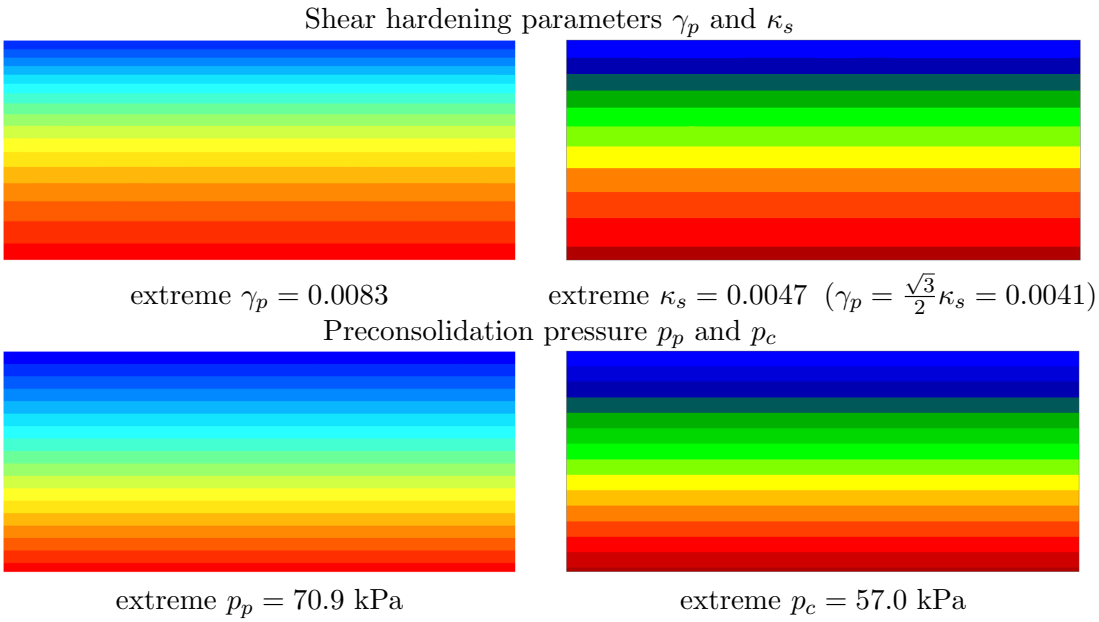


Figure 10: 1st calculation stage: comparison of hardening parameters generated by Plaxis (left) and GEO5 FEM for soil No. **5.2** (right)

Similarly to the Mohr-Coulomb model we summarize in Table 5 the evolution of vertical displacements associated with various sets of model parameters available in Tables 1 and 2. A graphical presentation is shown in Fig. 11.

Table 5: Settlement at the center of strip footing [mm]

| Calculation stage | Plaxis | GEO5 S**3** | GEO5 S**4** | GEO5 S**5.1** | GEO5 S**5.2** |
|---|---|---|---|---|---|
| Initial stresses | 0 | 0 | 0 | 0 | 0 |
| Surface surcharge of 20 kPa | 14.4 | 14.7 | 18.1 | 13.1 | 11.2 |
| Unloading | 9.7 | 10.5 | 13.1 | 8.8 | 7.6 |
| Strip footing self-weight | 15.2 | 15.3 | 18.9 | 13.6 | 11.6 |
| Uniform pressure of 200 kPa | 84.7 | 69.3 | 89.6 | 67.7 | 61.9 |

It is seen that the results essentially correspond to the predicted stress-strain diagrams derived from uniaxial compression test (oedometer), recall Figs. 4(a) and 5(a). The values at the end of the last calculation stage are bound by the estimates associated with model parameters of soil No. **5.2** (the stiffest response, black line in Fig. 11(a)) and soil No. **4** (the most compliant response, blue line in Fig. 11(b)). Point out that the graph is constructed by taking into account the values from Table 5 only. The actual variation of vertical displacements is, however, nonlinear owing to the evolution of plastic strains. To some extend, this is visible in Fig. 11(b) generated via the monitor option in GEO5 FEM.

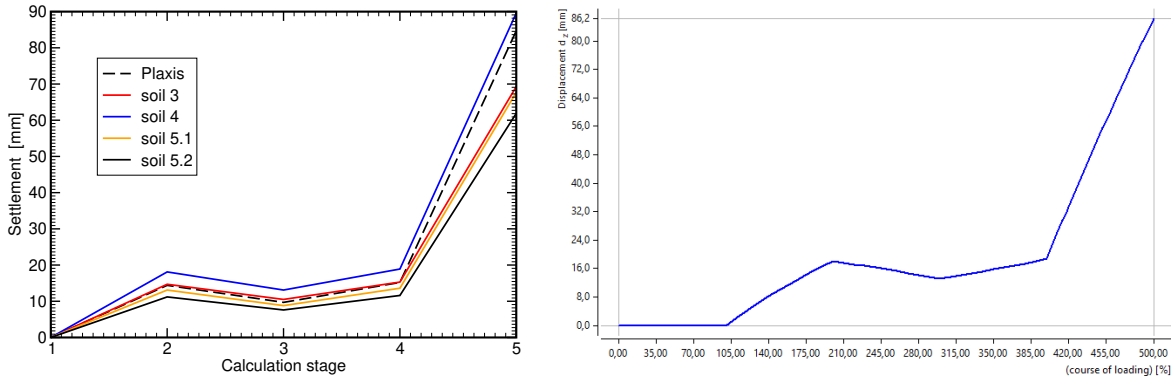


(a) (b)

Figure 11: a) Piecewise linear evolution of settlement at the center of strip footing with individual calculation stages, b) application of monitor option in GEO5 FEM

Additional illustrative comparisons are available in Figures 13 - 15. As with the previous surface plots we should keep in mind that colors may represent isosurfaces of different level. Regardless of that it is seen already in Fig. 13 that the Plaxis shear hardening parameter $\gamma_p$ experiences a higher degree of localization at the vicinity of beam end points in comparison to data provided by GEO5 FEM. This is further highlighted in Figs. 14 and 15 corresponding to the end of the final calculation stage. This applies also to the preconsolidation pressure $p_c$. However, the response predicted by both Plaxis and GEO5 FEM is qualitatively similar. The soil No. **3** is chosen in this particular study on purpose as the model parameters correspond to the case when the user adopts the input data directly from Plaxis and allows the program GEO5 FEM to estimate the cap parameters on the basis of the inputted values of $E_{oed}$ and $K_0^{NC}$. To appreciate a some what slower evolution of the preconsolidation pressure in soil No. **3** in comparison to soil No. **5.2** we plot the evolution of preconsolidation pressure $p_c$ in the isotropic compression test in Fig. 12 clearly showing the variation of $p_c$ in individual soils for the same value of strain.

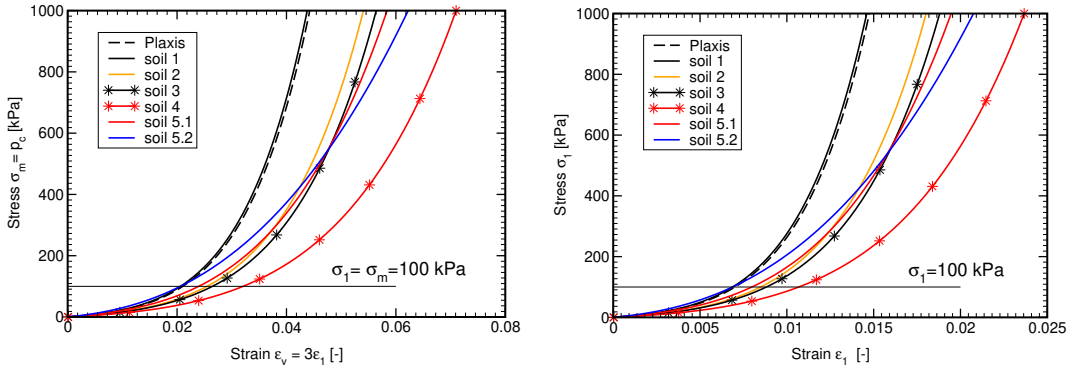


(a) (b)

Figure 12: Response in isotropic compression: a) $\sigma_m - \varepsilon_v$, b) $\sigma_1 - \varepsilon_1$

These plots also suggest that in the case of isotropic compression, where only the cap yield surface evolves, the two softwares perform identically, compare the solid and dashed black lines derived from the two softwares for the same set of data. Remind that this particular test excludes the effect of different stiffness formulation as $\sigma_m = \sigma_3$ in Eqs. (1) and (2).

Vertical displacements

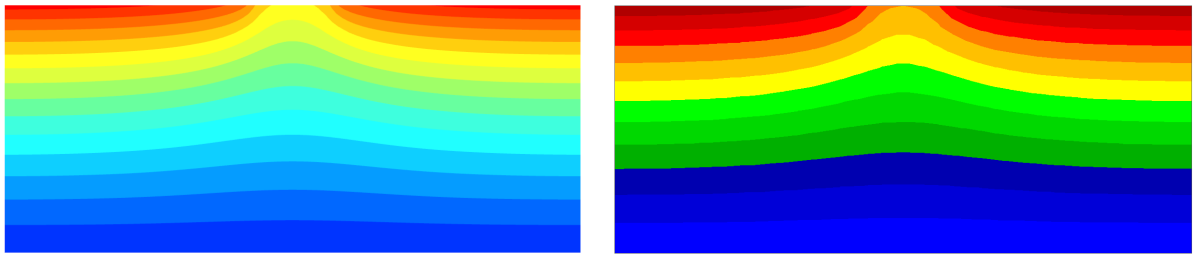

Equivalent deviatoric strains $\varepsilon_q$ and $E_d$

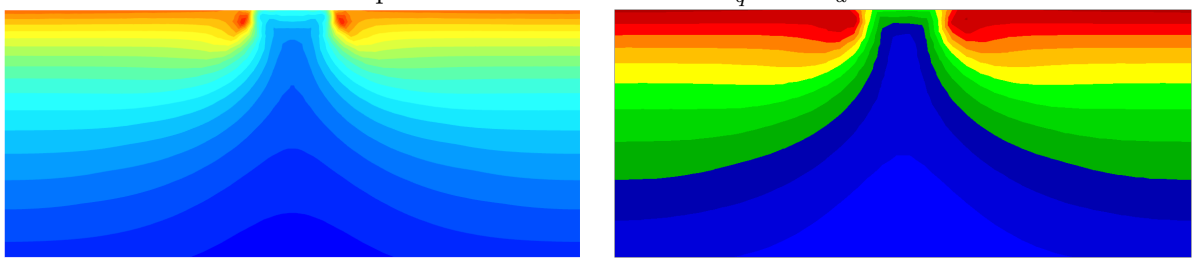

extreme $\varepsilon_q = 0.0065$ extreme $E_d = 0.0069$ $(\varepsilon_q = \frac{1}{\sqrt{3}} E_d = 0.0040)$

Shear hardening parameters $\gamma_p$ and $\kappa_s$

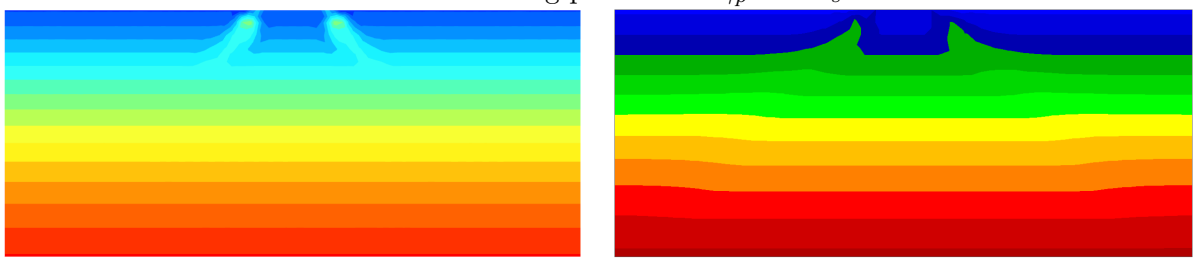

extreme $\gamma_p = 0.0092$ extreme $\kappa_s = 0.0054$ $(\gamma_p = \frac{\sqrt{3}}{2} \kappa_s = 0.0047)$

Preconsolidation pressure $p_p$ and $p_c$

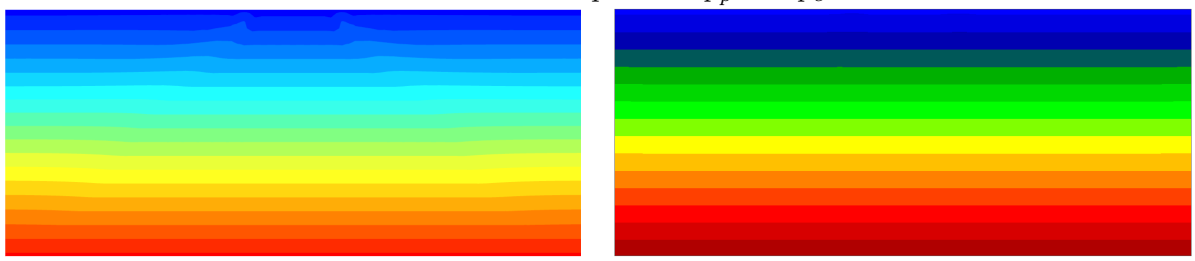

extreme $p_p = 93.0$ kPa extreme $p_c = 75.6$ kPa

Figure 13: 3rd calculation stage (unloading): comparison of selected outputs generated by Plaxis (left) and GEO5 FEM for soil No. **5.2** (right)

Strip displacements [mm]


Vertical displacements

Equivalent deviatoric strains $\varepsilon_q$ and $E_d$

extreme $\varepsilon_q = 0.1382$ extreme $E_d = 0.0682$ $(\varepsilon_q = \frac{1}{\sqrt{3}} E_d = 0.0394)$

Shear hardening parameters $\gamma_p$ and $\kappa_s$

extreme $\gamma_p = 0.2381$ extreme $\kappa_s = 0.0599$ $(\gamma_p = \frac{\sqrt{3}}{2} \kappa_s = 0.0519)$

Preconsolidation pressure $p_p$ and $p_c$

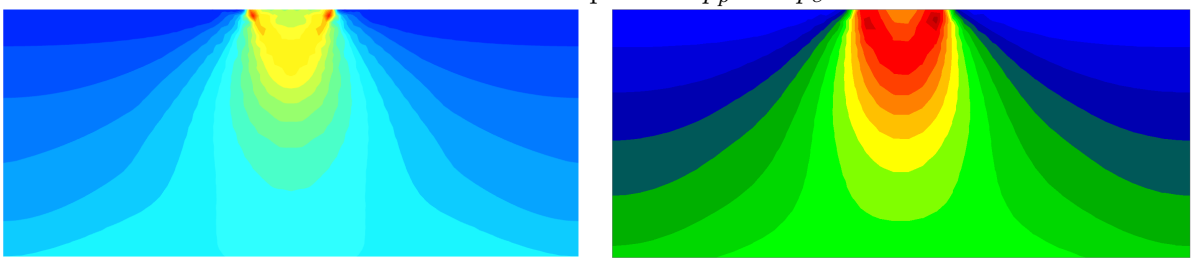

extreme $p_p = 382$ kPa extreme $p_c = 234$ kPa

Bending moment [kNm/m]

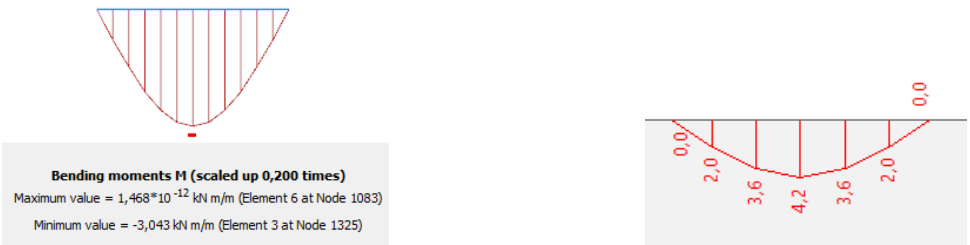


Figure 14: 5th calculation stage (footing loading): comparison of selected outputs generated by Plaxis (left) and GEO5 FEM for soil No. **5.2** (right)

Strip displacements [mm]

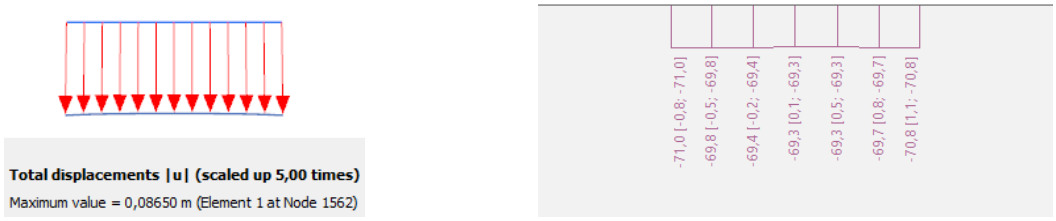


Vertical displacements

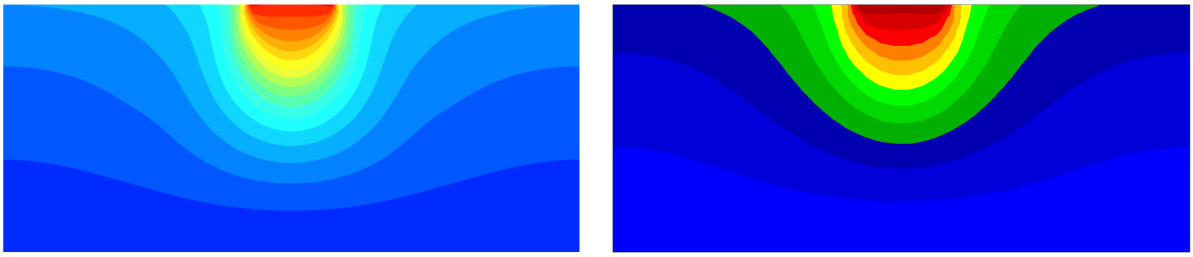

Equivalent deviatoric strains $\varepsilon_q$ and $E_d$

extreme $\varepsilon_q = 0.1382$ extreme $E_d = 0.0728$ $(\varepsilon_q = \frac{1}{\sqrt{3}} E_d = 0.0420)$

Shear hardening parameters $\gamma_p$ and $\kappa_s$

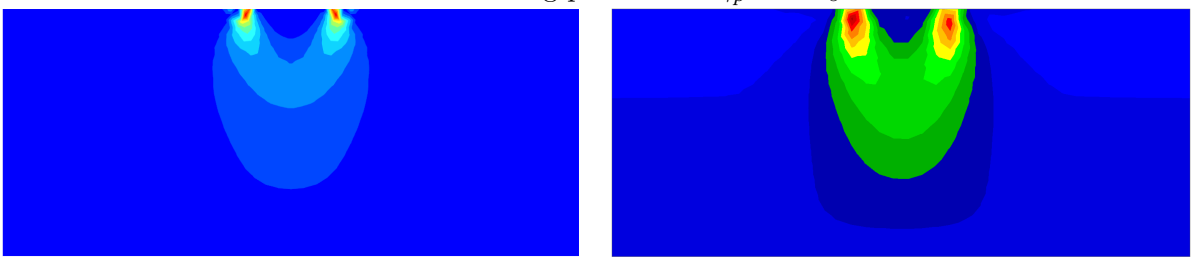

extreme $\gamma_p = 0.2381$ extreme $\kappa_s = 0.0684$ $(\gamma_p = \frac{\sqrt{3}}{2} \kappa_s = 0.0592)$

Preconsolidation pressure $p_p$ and $p_c$

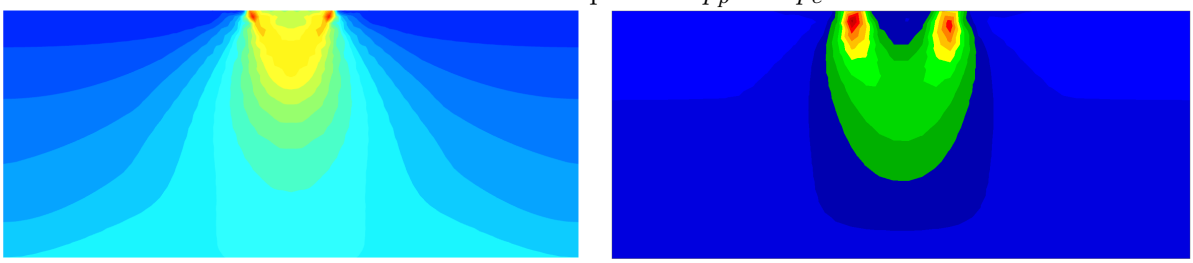

extreme $p_p = 382$ kPa extreme $p_c = 196$ kPa

Bending moment [kNm/m]

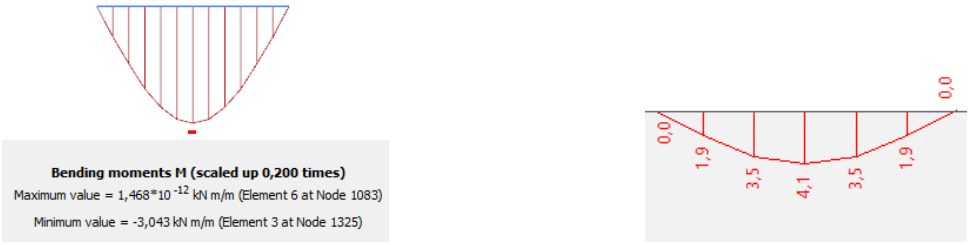


Figure 15: 5th calculation stage (footing loading): comparison of selected outputs generated by Plaxis (left) and GEO5 FEM for soil No. **3** (right)

# 5 Anchored retaining wall

The second example is concerned with the modeling of anchored retaining wall. This is a relatively complex task where the potential differences in the predicted behavior might be attributed not only to the formulation and implementation of the constitutive model but also to other issues including the finite element mesh, response of interface elements, application of anchors, etc. This is also why a careful preparation of a computational model plays an important role. Thus to minimize the influence of various structural elements we first tuned the computational model by simulating the entire excavation process considering a homogeneous subsoil of the Mohr-Coulomb type. The resulting finite element meshes appear in Fig. 16. Note that a beam element with an *elephant foot* is used in GEO5 FEM to prevent excessive vertical displacement of a sheeting wall. Similar action was expected in Plaxis by choosing the *Prevent punching* option.

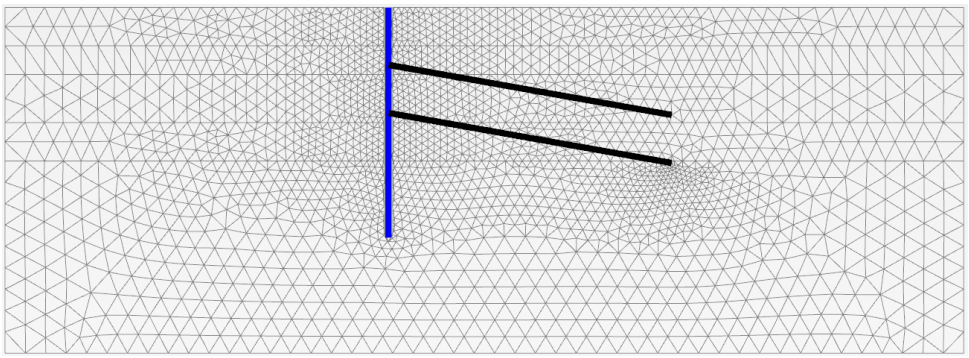

(a)

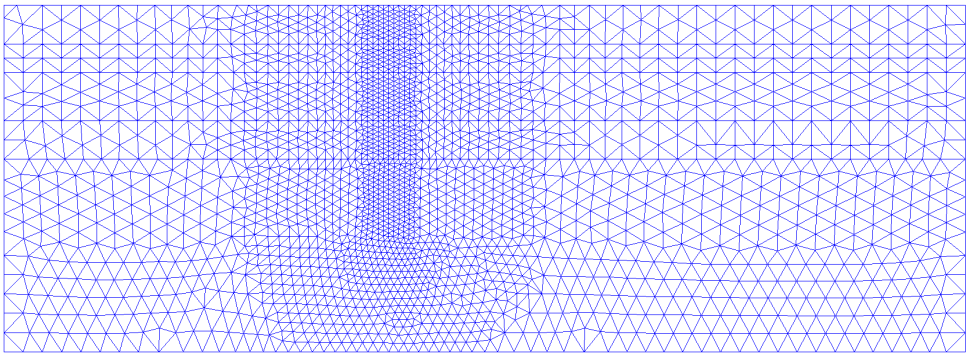

(b)

Figure 16: 6-noded triangular elements with edge size of about 1 m and further refined near the wall to about 0.25 m - 0.35 m: a) Plaxis, b) GEO5 FEM

The modeling strategy proceeded along the following lines:

1. The $K_0$ procedure was used again to generate the initial stress which easily allows us to initialize the hardening parameters of Hardening soil model.
2. The retaining wall was installed in the 2nd construction stage introducing an additional surcharge due to the wall self-weight.
3. The remaining construction sequence considered several excavation and anchoring steps starting with the 1st excavation step up to a depth of 3.5 m.
4. The first row of anchors was installed and the anchors were prestressed to the value of 150 kN.
5. Excavation up to a depth of 6 m proceeded next.
6. The second row of anchors was installed and the anchors were prestressed again to the value of 150 kN.
7. The final construction stage considered excavation up to a depth of 8 m.

### 5.1 Simulation with Mohr-Coulomb model

A homogeneous soil of the Mohr-Coulomb type with the model parameters taken from Table 3 was considered. The results obtained at individual construction stages starting from the 1st excavation step are summarized in Tables 6 - 10. A reasonable agreement of the selected results is observed. This is supported by surface plots of horizontal and vertical displacements in Figs. 17 and 18 and also by a graphical representation of bending moments in Fig. 19. All this promotes the application of the designed computational models in the simulation of the same task with the Hardening soil model.

Table 6: Stage No. 3: excavation up to depth of 3.5 m

| | Plaxis | GEO5 |
|---|---|---|
| Heave of the pit bottom [mm] | 46.0 | 44.4 |
| Horizontal displ. wall top [mm] | 8.0 | 7.3 |
| Horizontal displ. wall bottom [mm] | 3.6 | 3.8 |
| Vertical displ. wall bottom [mm] | 2.7 | 2.5 |
| Extreme bending moment [kNm/m] | 49.6 | 43.2 |

Table 7: Stage No. 4: installation of 1st row of anchors

| | Plaxis | GEO5 |
|---|---|---|
| Heave of the pit bottom [mm] | 46.1 | 44.4 |
| Horizontal displ. wall top [mm] | 2.8 | 2.4 |
| Horizontal displ. wall bottom [mm] | 4.0 | 3.9 |
| Vertical displ. wall bottom [mm] | 3.4 | 2.2 |
| Extreme bending moment [kNm/m] | 53.4 | 51.9 |
| Anchor forces [kN/m] | 150 | 150 |

Table 8: Stage No. 5: excavation up to depth of 6 m

| | Plaxis | GEO5 |
|---|---|---|
| Heave of the pit bottom [mm] | 65.3 | 63.9 |
| Horizontal displ. wall top [mm] | 13.0 | 11.2 |
| Horizontal displ. wall bottom [mm] | 5.7 | 6.2 |
| Vertical displ. wall bottom [mm] | 2.3 | 5.3 |
| Extreme bending moment [kNm/m] | 45.0 | 51.4 |
| Anchor forces [kN/m] | 179 | 182 |

Table 9: Stage No. 6: installation of 2nd row of anchors

| | Plaxis | GEO5 |
|---|---|---|
| Heave of the pit bottom [mm] | 65.3 | 63.9 |
| Horizontal displ. wall top [mm] | 10.6 | 9.0 |
| Horizontal displ. wall bottom [mm] | 5.3 | 5.8 |
| Vertical displ. wall bottom [mm] | 3.0 | 5.0 |
| Extreme bending moment [kNm/m] | 50.1 | 42.1 |
| Anchor forces [kN/m] | 163/150 | 166/150 |

Table 10: Stage No. 7: excavation up to depth of 8 m

| | Plaxis | GEO5 |
|---|---|---|
| Heave of the pit bottom [mm] | 72.3 | 71.1 |
| Horizontal displ. wall top [mm] | 20.8 | 17.2 |
| Horizontal displ. wall bottom [mm] | 7.6 | 8.4 |
| Vertical displ. wall bottom [mm] | 7.9 | 3.7 |
| Extreme bending moment [kNm/m] | 120.2 | 128.1 |
| Anchor forces [kN/m] | 189/161 | 192/178 |

Stage No. 3: excavation up to depth of 3.5 m

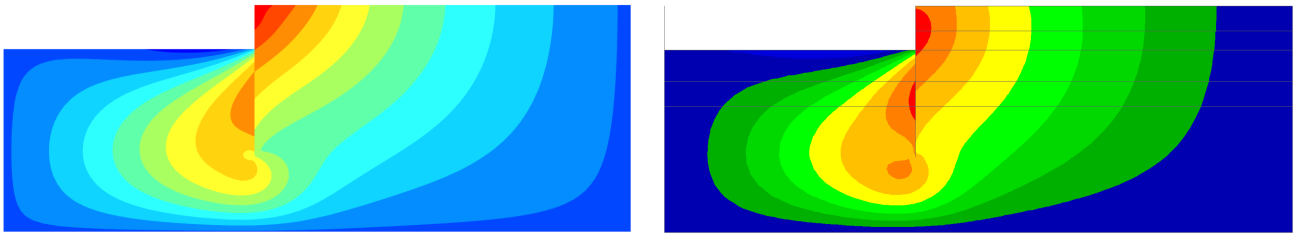

Stage No. 6: installation of 2nd row of anchors

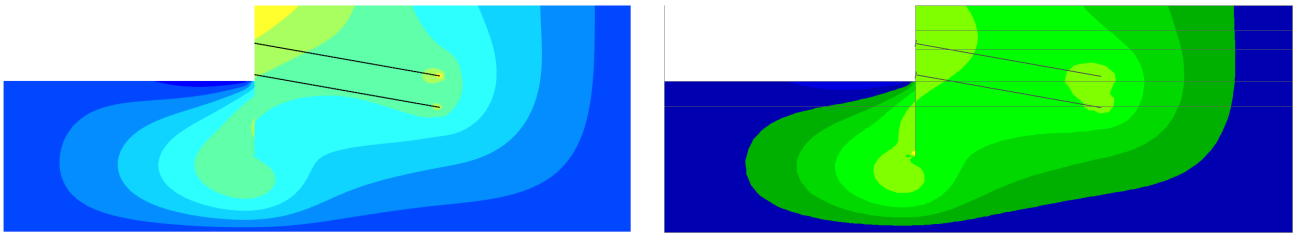

Stage No. 7: excavation up to depth of 8 m

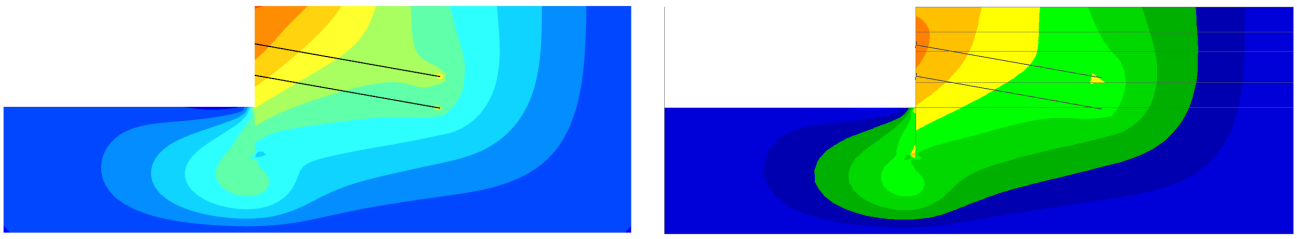

Figure 17: Comparison of **horizontal displacements**: Plaxis (left), GEO5 FEM (right)

Stage No. 3: excavation up to depth of 3.5 m

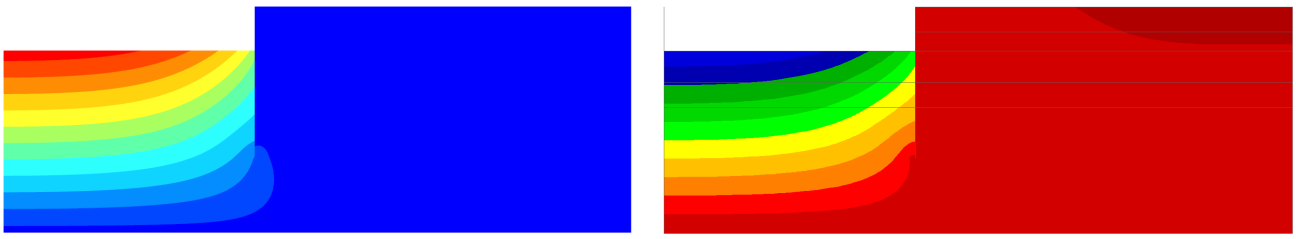

Stage No. 6: installation of 2nd row of anchors

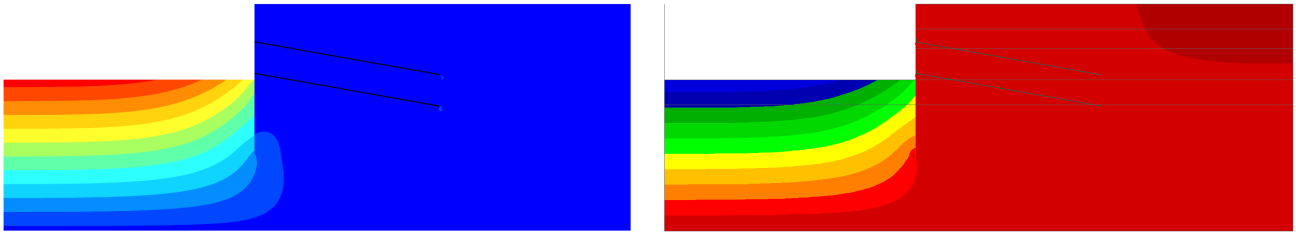

Stage No. 7: excavation up to depth of 8 m

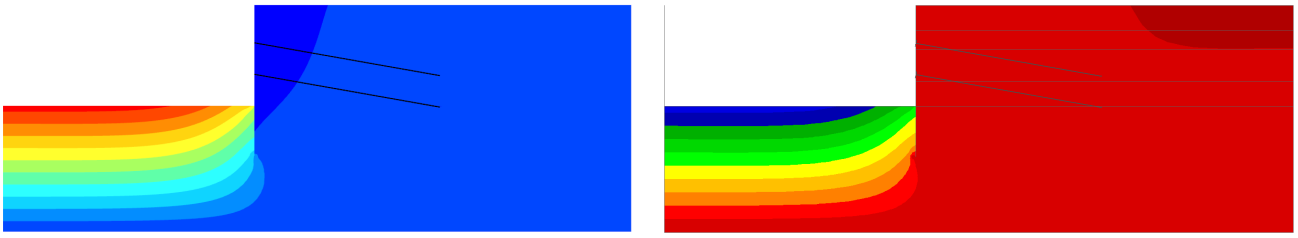

Figure 18: Comparison of **vertical displacements**: Plaxis (left), GEO5 FEM (right)

Stage No. 3: excavation up to depth of 3.5 m

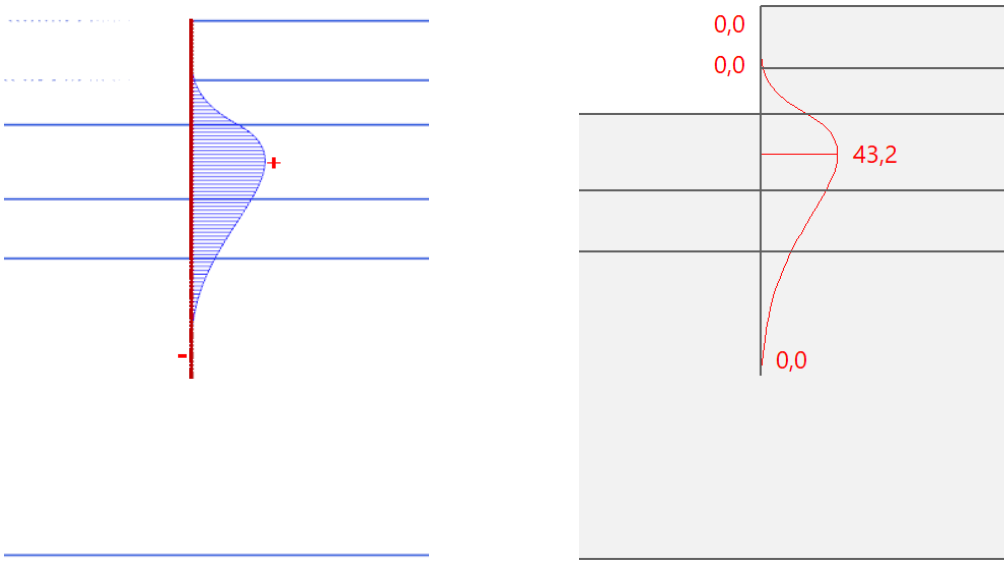


Stage No. 6: installation of 2nd row of anchors

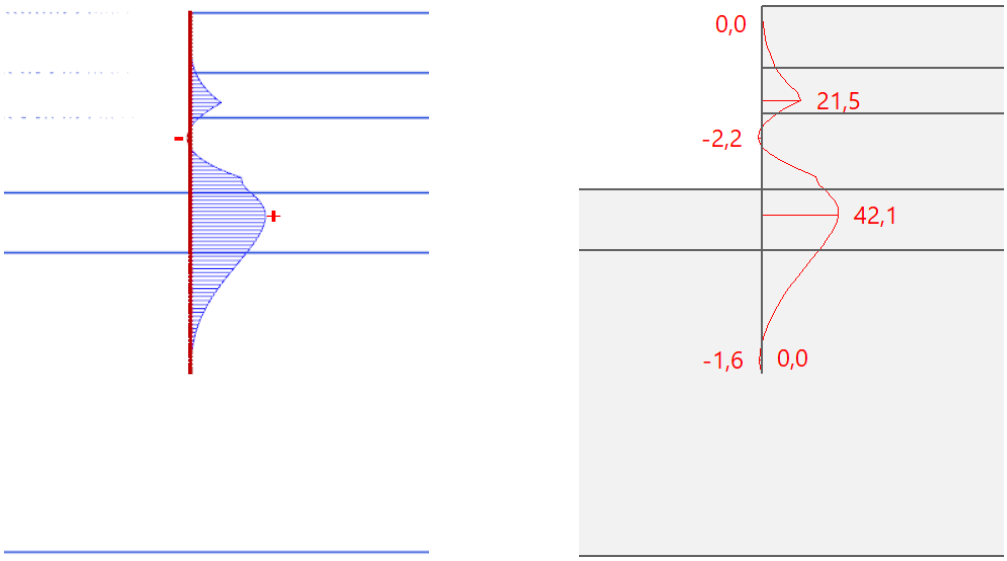


Stage No. 7: excavation up to depth of 8 m

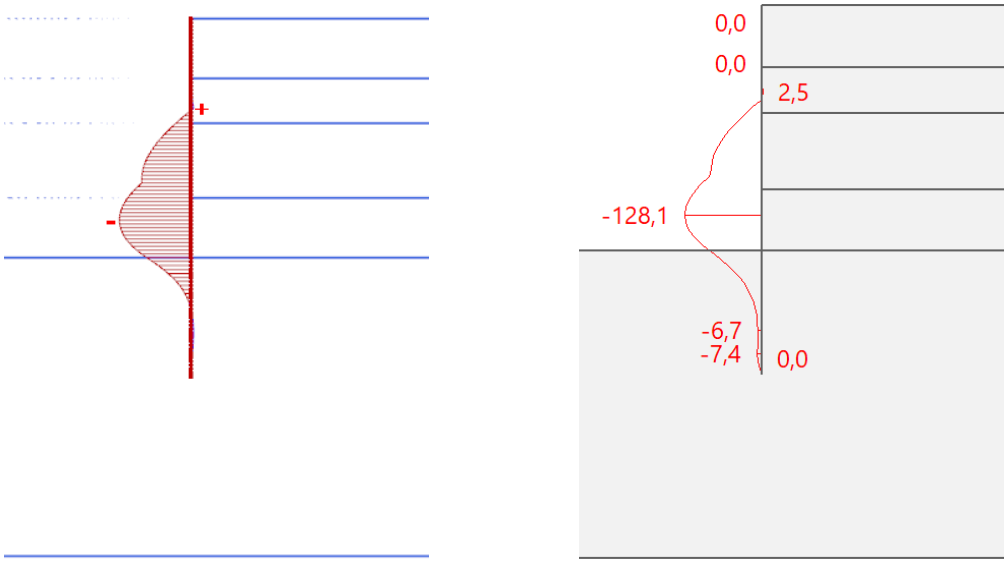


Figure 19: Comparison of **bending moments**: Plaxis (left), GEO5 FEM (right)

### 5.2 Simulation with Hardening soil model

We start from the results summarized in Tables 11 - 15. In terms of displacements, the general conclusions drawn for the case of strip footing in light of the examined sets of model parameters apply also to this example. The most compliant response is again observed for soil No. **4** but in terms of horizontal displacements this response is still considerably stiffer in comparison to Plaxis predictions. This is even more pronounced for other sets of data confirming the soil No. **5.2** to yield the stiffest response. Nevertheless, the difference between the two software predictions is relatively mild up to the 6th calculation stage but amounting to almost 50% at the end of the last calculation stage. However, in terms of heave of the pit bottom the difference in vertical displacements is negligible. A qualitative similarity in the displacement field is further shown in Figs. 20 and 21. But recall that the colors identifying individual isosurfaces do not again correspond to the same values.

Table 11: Stage No. 3: excavation up to depth of 3.5 m

| | Plaxis | G5 S**3** | G5 S**4** | G5 S**5.1** | G5 S**5.2** |
|---|---|---|---|---|---|
| Heave of the pit bottom [mm] | 49.6 | 39.4 | 49.0 | 46.0 | 45.4 |
| Horizontal displ. wall top [mm] | 17.1 | 12.8 | 13.7 | 12.9 | 12.4 |
| Horizontal displ. wall bottom [mm] | 2.2 | 1.8 | 2.4 | 2.4 | 2.6 |
| Vertical displ. wall bottom [mm] | 9.7 | 2.7 | 2.9 | 2.2 | 2.2 |
| Extreme bending moment [kNm/m] | 56.2 | 51.8 | 49.0 | 48.4 | 49.8 |

Table 12: Stage No. 4: installation of 1st row of anchors

| | Plaxis | G5 S**3** | G5 S**4** | G5 S**5.1** | G5 S**5.2** |
|---|---|---|---|---|---|
| Heave of the pit bottom [mm] | 49.6 | 39.4 | 49.0 | 46.0 | 45.4 |
| Horizontal displ. wall top [mm] | 8.9 | 7.1 | 7.4 | 6.9 | 6.6 |
| Horizontal displ. wall bottom [mm] | 3.1 | 2.0 | 2.6 | 2.5 | 2.8 |
| Vertical displ. wall bottom [mm] | 10.5 | 2.9 | 3.1 | 2.4 | 2.5 |
| Extreme bending moment [kNm/m] | 34.7 | 50.0 | 52.6 | 51.7 | 51.6 |
| Anchor forces [kN/m] | 150 | 150 | 150 | 150 | 150 |

Table 13: Stage No. 5: excavation up to depth of 6 m

| | Plaxis | G5 S**3** | G5 S**4** | G5 S**5.1** | G5 S**5.2** |
|---|---|---|---|---|---|
| Heave of the pit bottom [mm] | 64.1 | 52.1 | 65.1 | 61.6 | 62.1 |
| Horizontal displ. wall top [mm] | 33.5 | 20.5 | 22.1 | 20.9 | 20.5 |
| Horizontal displ. wall bottom [mm] | 4.1 | 3.3 | 4.3 | 4.2 | 4.6 |
| Vertical displ. wall bottom [mm] | 13.8 | 2.3 | 2.0 | 1.3 | 1.1 |
| Extreme bending moment [kNm/m] | 72.6 | 64.7 | 64.9 | 64.7 | 64.2 |
| Anchor forces [kN/m] | 201 | 192 | 194 | 193 | 192 |

Table 14: Stage No. 6: installation of 2nd row of anchors

| | Plaxis | G5 S**3** | G5 S**4** | G5 S**5.1** | G5 S**5.2** |
|---|---|---|---|---|---|
| Heave of the pit bottom [mm] | 64.1 | 52.1 | 65.1 | 61.6 | 62.1 |
| Horizontal displ. wall top [mm] | 29.0 | 17.8 | 19.0 | 18.0 | 17.8 |
| Horizontal displ. wall bottom [mm] | 4.1 | 3.1 | 4.0 | 3.9 | 4.3 |
| Vertical displ. wall bottom [mm] | 14.6 | 2.5 | 2.2 | 1.5 | 1.4 |
| Extreme bending moment [kNm/m] | 37.6 | 35.4 | 37.6 | 36.2 | 38.1 |
| Anchor forces [kN/m] | 178/150 | 175/150 | 175/150 | 174/150 | 174/150 |

Table 15: Stage No. 7: excavation up to depth of 8 m

| | Plaxis | G5 S**3** | G5 S**4** | G5 S**5.1** | G5 S**5.2** |
|---|---|---|---|---|---|
| Heave of the pit bottom [mm] | 68.3 | 55.8 | 69.8 | 66.3 | 67.4 |
| Horizontal displ. wall top [mm] | 62.9 | 30.4 | 33.1 | 31.4 | 31.4 |
| Horizontal displ. wall bottom [mm] | 8.7 | 5.7 | 6.9 | 6.8 | 7.4 |
| Vertical displ. wall bottom [mm] | 29.7 | 5.3 | 5.4 | 4.6 | 4.5 |
| Extreme bending moment [kNm/m] | 198.3 | 161.4 | 161.0 | 161.0 | 160.5 |
| Anchor forces [kN/m] | 251/186 | 214/189 | 215/190 | 214/189 | 213/189 |

Stage No. 3: excavation up to depth of 3.5 m

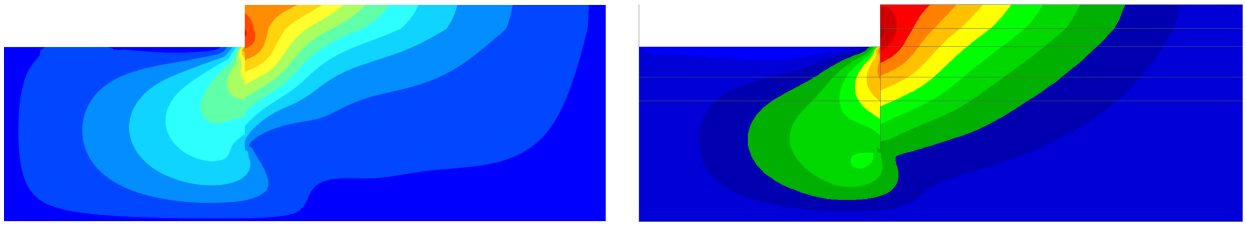

Stage No. 6: installation of 2nd row of anchors

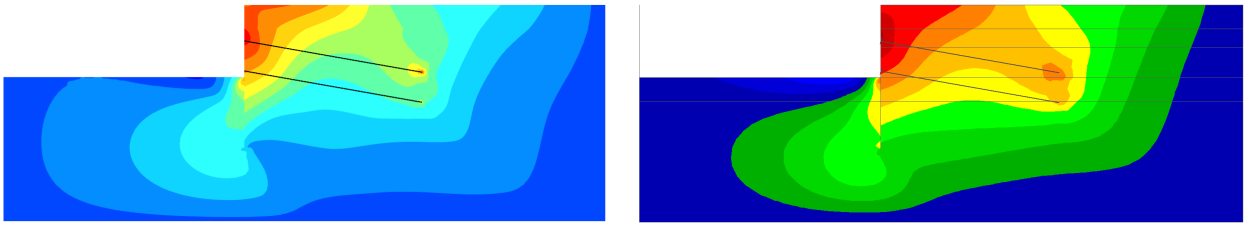

Stage No. 7: excavation up to depth of 8 m

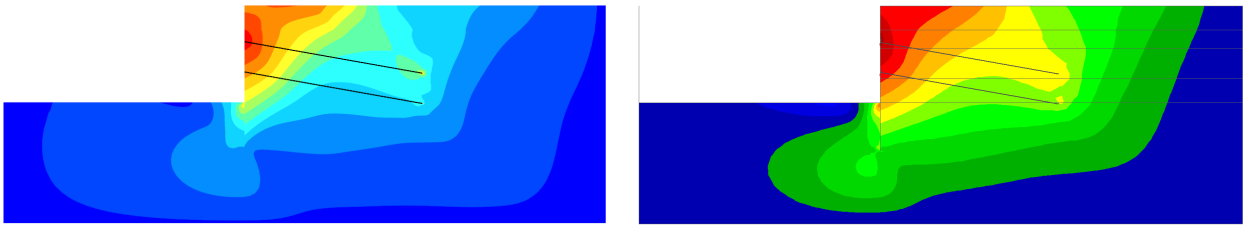

Figure 20: Comparison of **horizontal displacements**: Plaxis (left), GEO5 FEM soil No. **5.2** (right)

Stage No. 3: excavation up to depth of 3.5 m

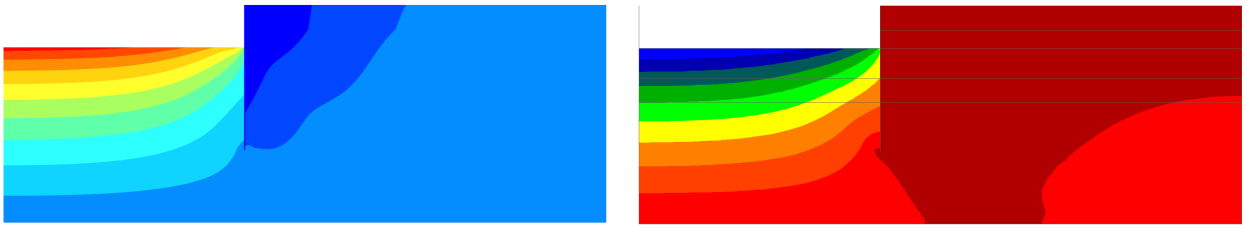

Stage No. 6: installation of 2nd row of anchors

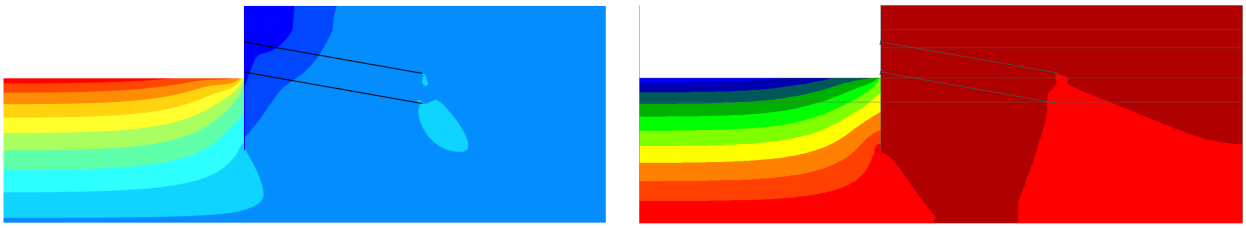

Stage No. 7: excavation up to depth of 8 m

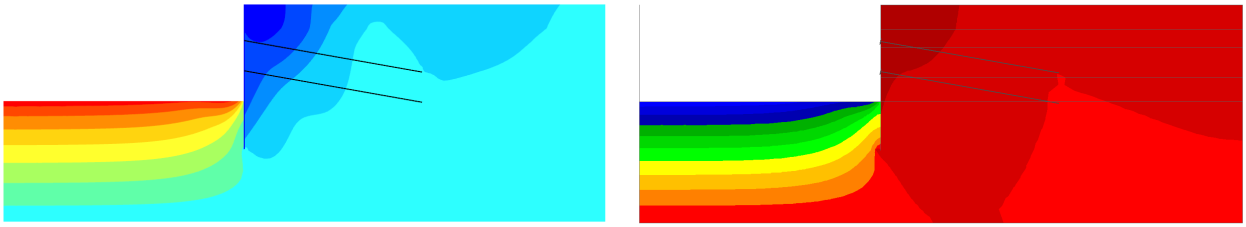

Figure 21: Comparison of **vertical displacements**: Plaxis (left), GEO5 FEM soil No. **5.2** (right)

**Stage No. 6: installation of 2nd row of anchors**

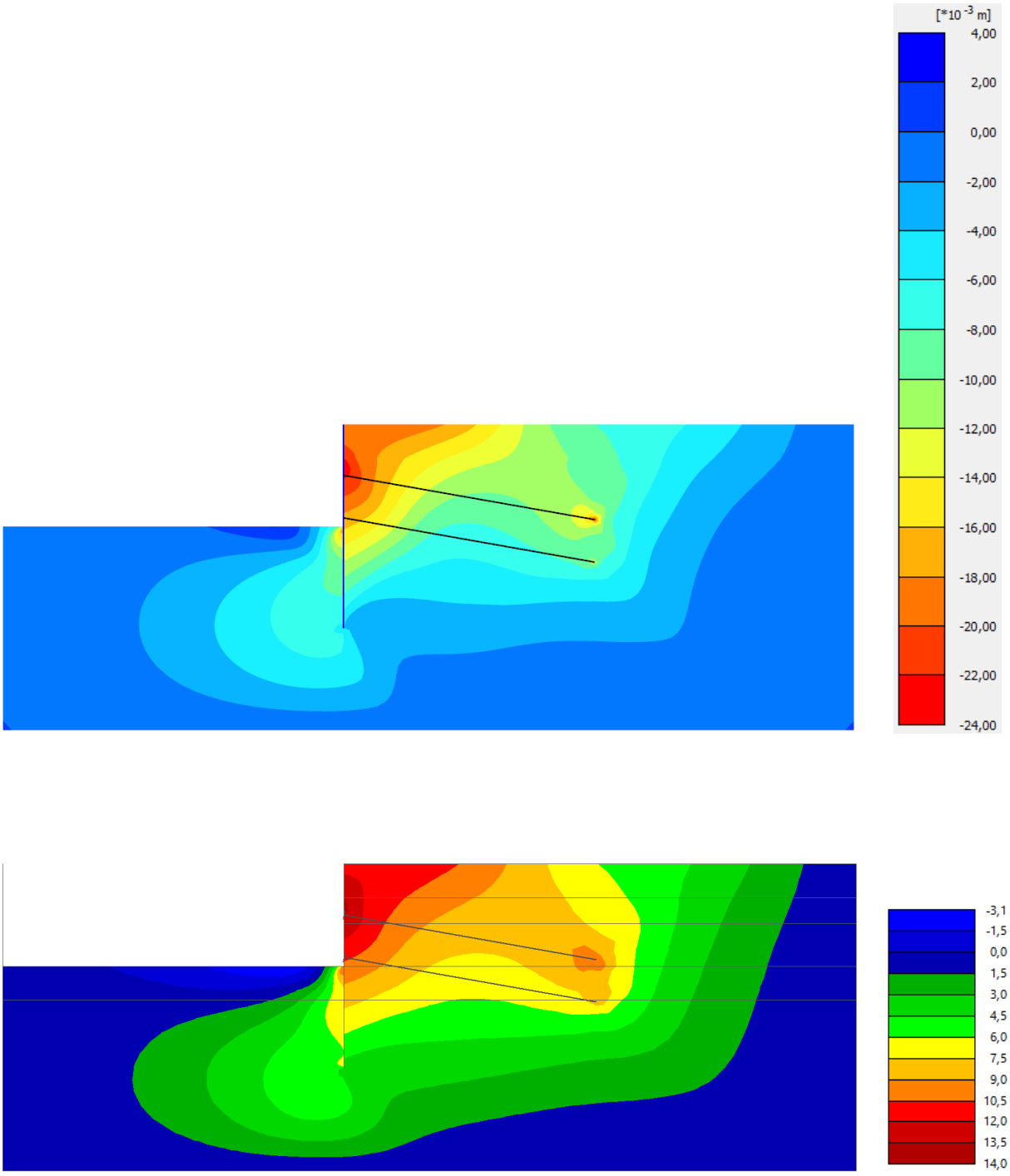


Figure 22: Comparison of **horizontal displacements**: Plaxis (top), GEO5 FEM soil No. **5.2** (bottom, displacements are in [mm])

**Stage No. 7: excavation up to depth of 8 m**

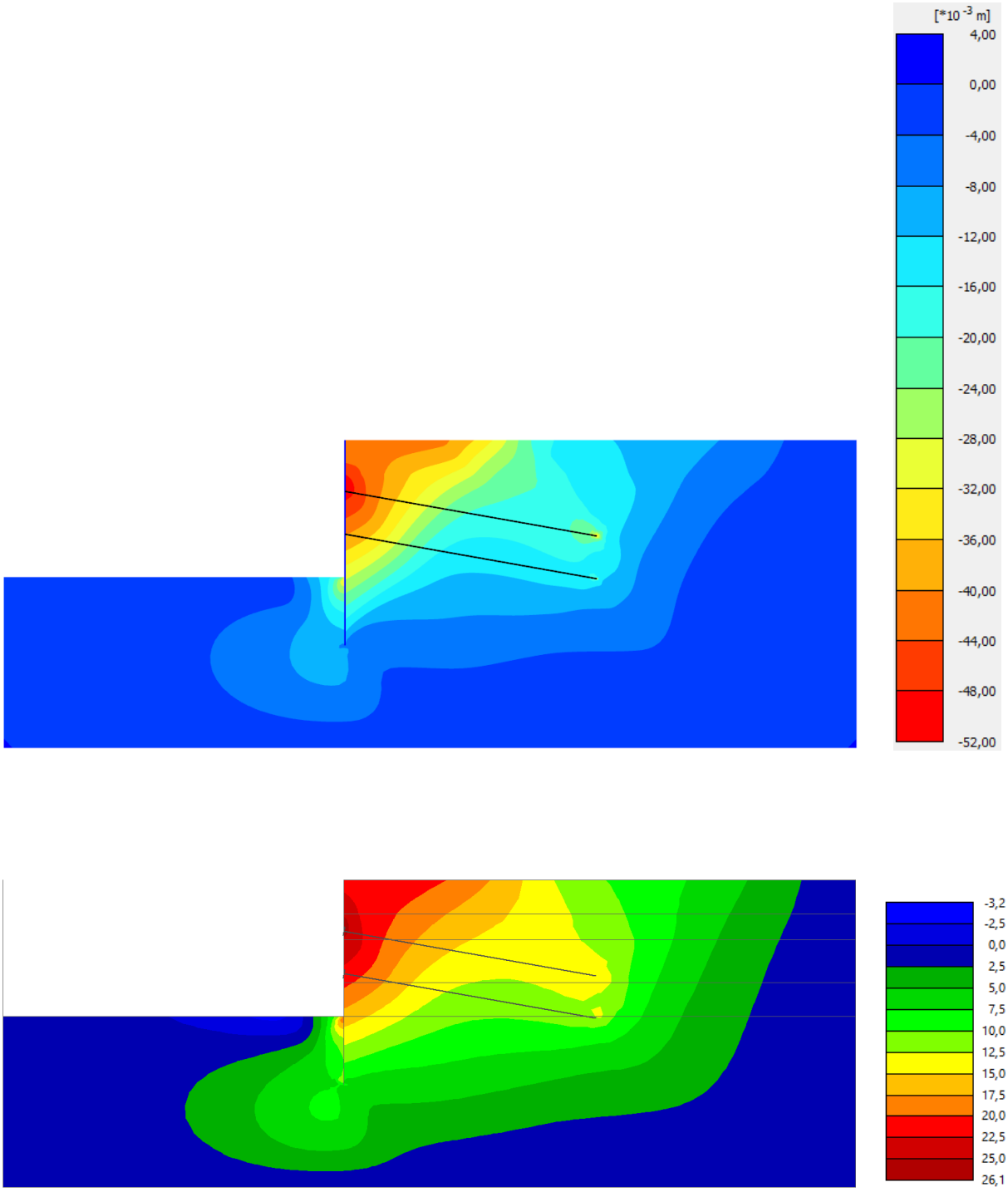


Figure 23: Comparison of **horizontal displacements**: Plaxis (top), GEO5 FEM soil No. **5.2** (bottom, displacements are in [mm])

Stage No. 3: excavation up to depth of 3.5 m

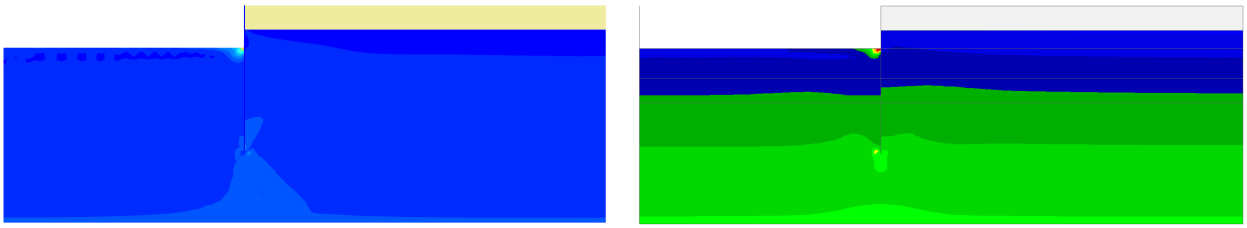

Stage No. 6: installation of 2nd row of anchors

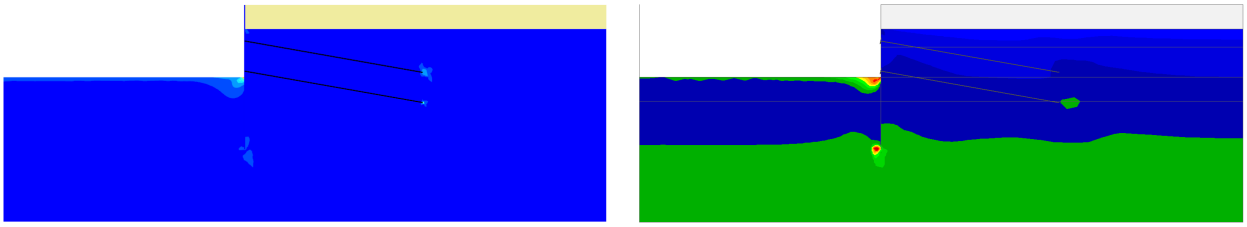

Stage No. 7: excavation up to depth of 8 m

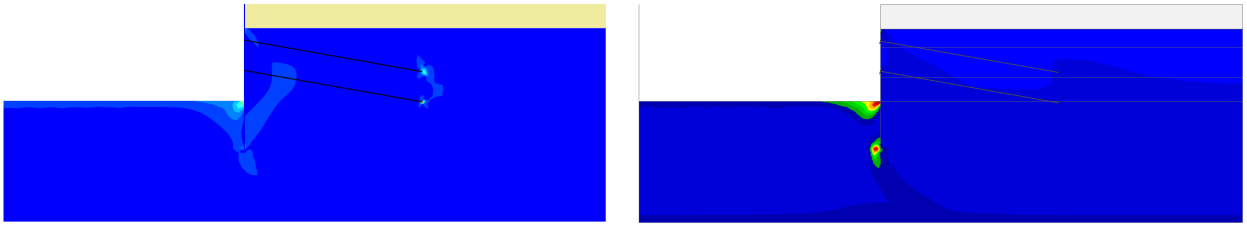

extreme $\gamma_p = 0.2577$ extreme $\kappa_s = 0.0517 (\gamma_p = \frac{\sqrt{3}}{2}\kappa_s = 0.0448)$

Figure 24: Comparison of **shear harden. parameter**: Plaxis (left), GEO5 FEM soil No. **5.2** (right)

Stage No. 3: excavation up to depth of 3.5 m

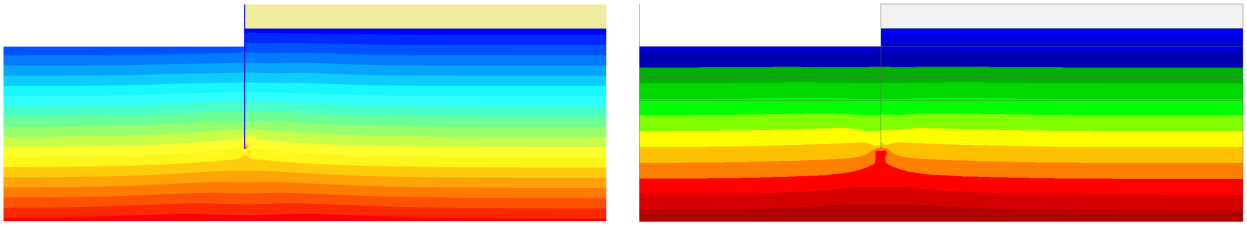

Stage No. 6: installation of 2nd row of anchors

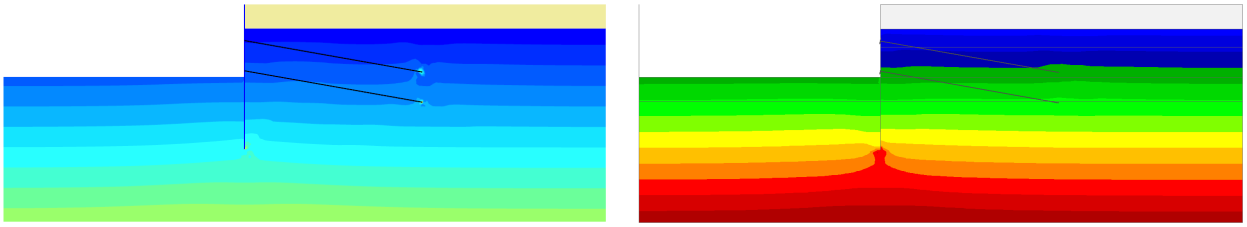

Stage No. 7: excavation up to depth of 8 m

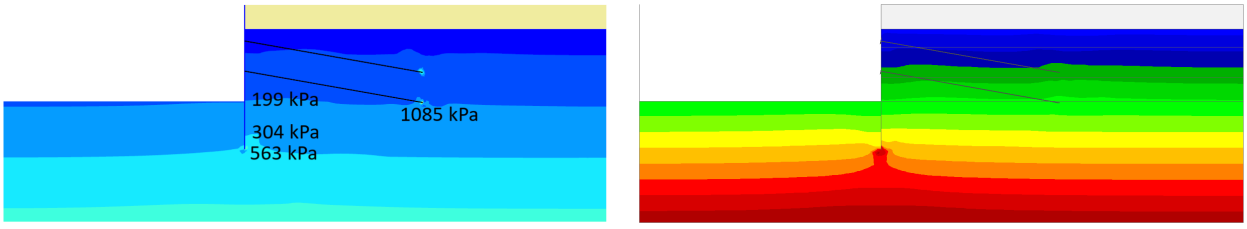


extreme $p_p = 1085$ kPa extreme $p_c = 350$ kPa

Figure 25: Comparison of **preconsolidation pressure**: Plaxis (left), GEO5 FEM soil No. **5.2** (right)

Stage No. 3: excavation up to depth of 3.5 m

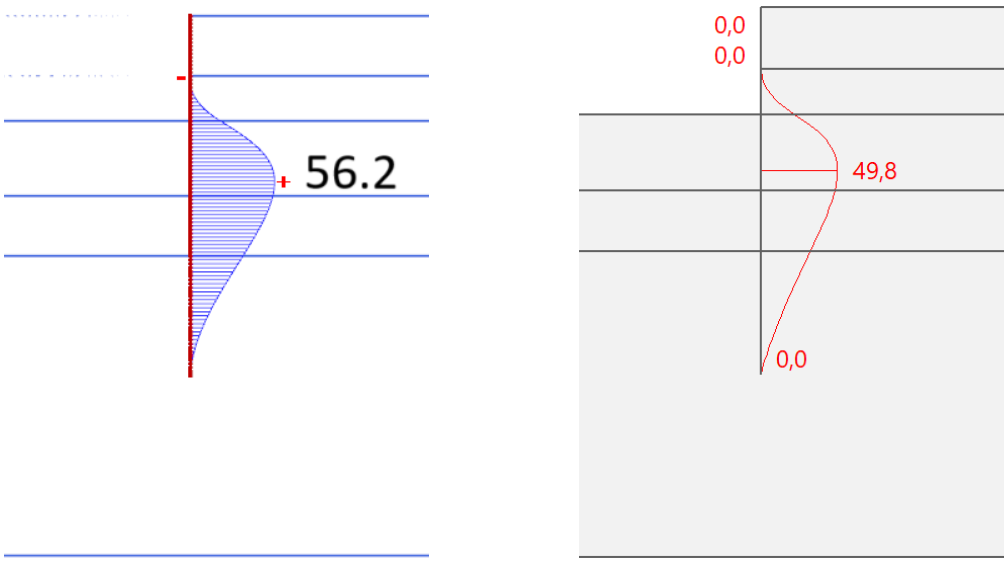


Stage No. 6: installation of 1st row of anchors

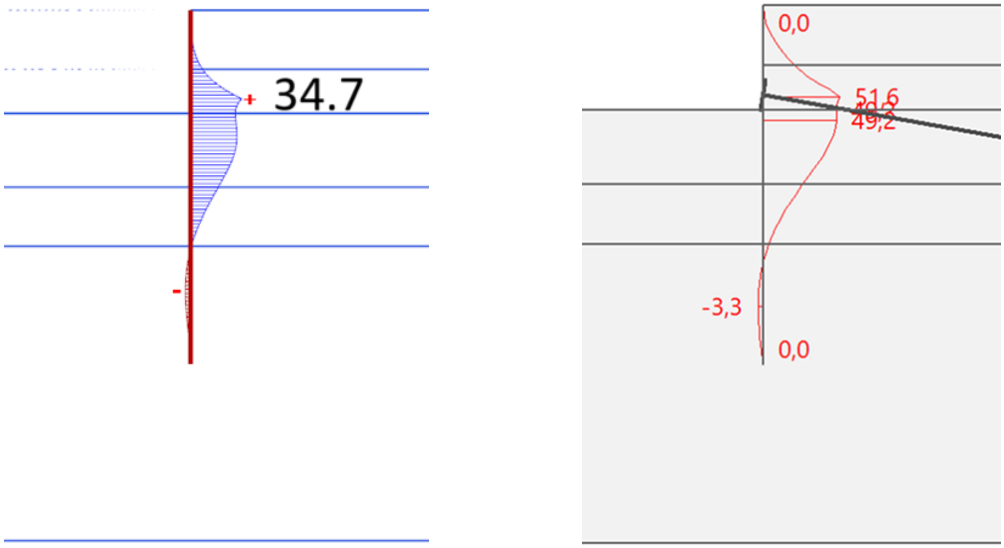


Stage No. 7: excavation up to depth of 6 m

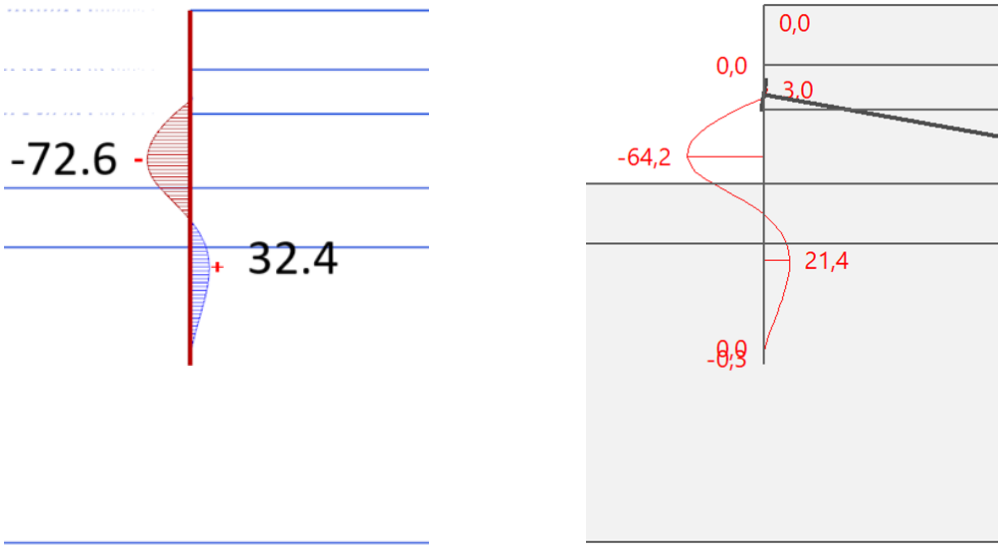


Figure 26: Comparison of **bending moments**: Plaxis (left), GEO5 FEM soil No. **5.2** (right)

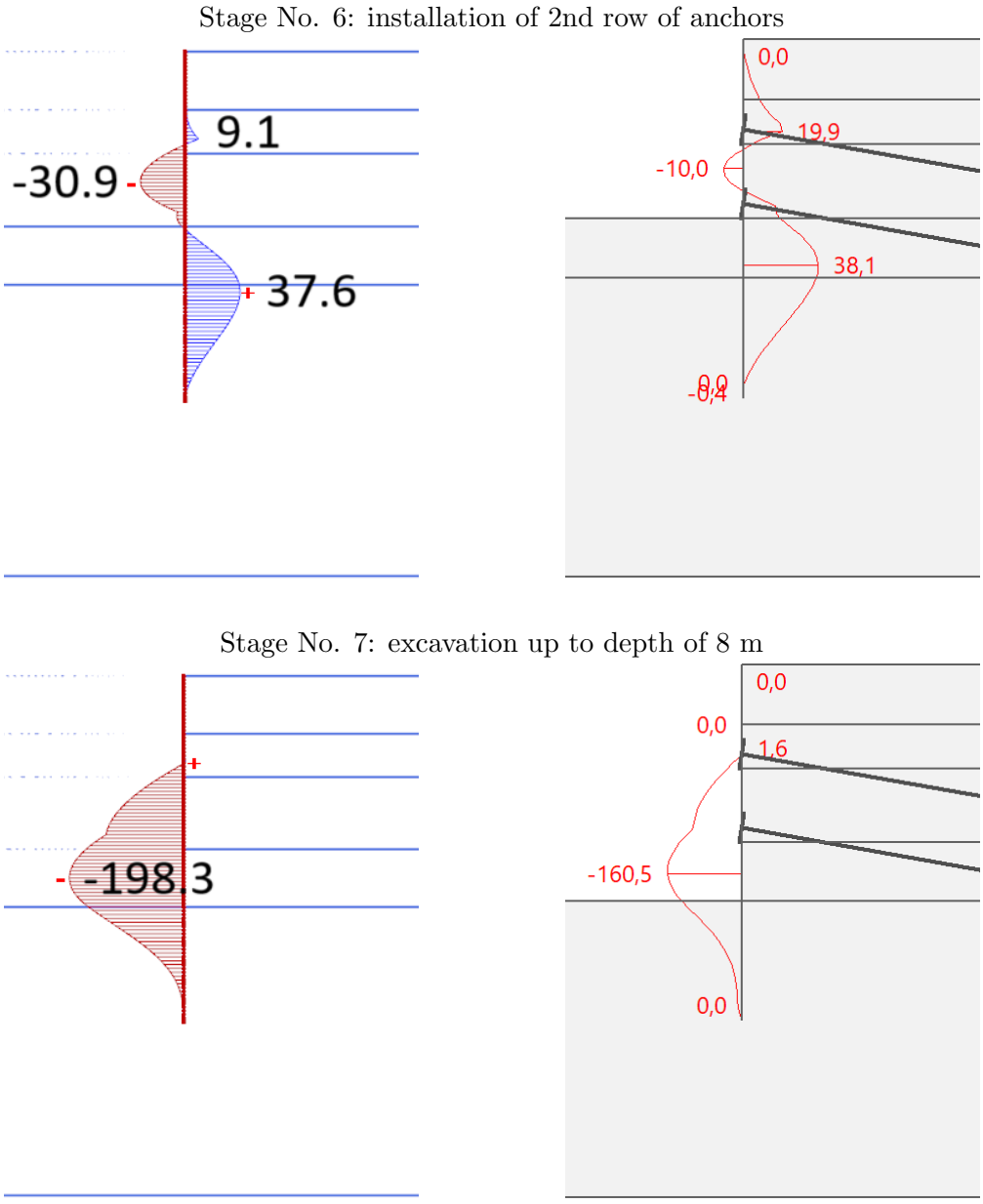


Figure 27: Comparison of **bending moments**: Plaxis (left), GEO5 FEM soil No. **5.2** (right)

Comparable predictions are available also for anchor forces. Here it is perhaps useful to mention that point-to-point anchors were adopted in this study. As seen Fig. 16(a), the Plaxis software assumes both end points be attached to a node of the underlying finite element mesh thus offering a relatively compliant representation of an anchor root. This is not the case in GEO5 FEM where the anchor response is mostly controlled by the displacements of nodes of an element with which the corresponding anchor end point is associated. This allows for modeling the *root* like part of the anchor more reasonably. The consequence of this difference is clearly visible from the distribution of shear hardening parameter and preconsolidation pressure in the vicinity of an anchor *root* end point in Figs. 24 and 25, respectively. Point out the location of extreme value of preconsolidation pressure provided by Plaxis in Fig. 25(a).

Next, we turn our attention to the evolution of bending moments across individual calculation stages. Similarly to other examined variables, no significant deviation appears when comparing the predictions provided by GEO5 FEM for individual sets of data parameters. Also, when compared to Plaxis, the results up to the 6th calculation stage match reasonably well, at least from the engineering point of view. A noticeable difference is evident for the last calculation stage where the maximum bending moment predicted by GEO5 FEM amounts to about 80% of that suggested by Plaxis.

Final observation is concerned with the vertical settlement of the sheeting wall. While in GEO5 FEM the *elephant foot* considerably reduces the evolution of vertical displacements, the *Prevent punching* option does not suggest a similar behavior as therein the vertical displacement continuously increases to values considerably higher in comparison to GEO5 FEM predictions, recall Tables 11 - 15. To see whether this might have an impact on other tracked parameters, we performed all the simulations with GEO5 FEM while replacing the foot-end with a hinge-end point of the beam element. The corresponding results are listed in Tables 16 - 20.

Table 16: Stage No. 3: excavation up to depth of 3.5 m, hinge-end point at wall bottom

| | Plaxis | G5 S**3** | G5 S**4** | G5 S**5.1** | G5 S**5.2** |
|---|---|---|---|---|---|
| Heave of the pit bottom [mm] | 49.6 | 39.3 | 49.0 | 45.9 | 45.4 |
| Horizontal displ. wall top [mm] | 17.1 | 13.5 | 14.3 | 13.5 | 13.1 |
| Horizontal displ. wall bottom [mm] | 2.2 | 1.4 | 2.0 | 2.0 | 2.2 |
| Vertical displ. wall bottom [mm] | 9.7 | 10.0 | 9.8 | 9.0 | 8.9 |
| Extreme bending moment [kNm/m] | 56.2 | 56.3 | 53.7 | 53.4 | 55.0 |

Table 17: Stage No. 4: installation of 1st row of anchors, hinge-end point at wall bottom

| | Plaxis | G5 S**3** | G5 S**4** | G5 S**5.1** | G5 S**5.2** |
|---|---|---|---|---|---|
| Heave of the pit bottom [mm] | 49.6 | 39.4 | 49.0 | 46.0 | 44.5 |
| Horizontal displ. wall top [mm] | 8.9 | 7.7 | 7.9 | 7.4 | 7.2 |
| Horizontal displ. wall bottom [mm] | 3.1 | 1.9 | 2.5 | 2.5 | 2.7 |
| Vertical displ. wall bottom [mm] | 10.5 | 10.5 | 10.4 | 9.6 | 9.5 |
| Extreme bending moment [kNm/m] | 34.7 | 54.1 | 56.4 | 55.6 | 56.2 |
| Anchor forces [kN/m] | 150 | 150 | 150 | 150 | 150 |

Table 18: Stage No. 5: excavation up to depth of 6 m, hinge-end point at wall bottom

| | Plaxis | G5 S**3** | G5 S**4** | G5 S**5.1** | G5 S**5.2** |
|---|---|---|---|---|---|
| Heave of the pit bottom [mm] | 64.1 | 52.1 | 65.0 | 61.5 | 62.0 |
| Horizontal displ. wall top [mm] | 33.5 | 22.8 | 24.2 | 23.0 | 22.8 |
| Horizontal displ. wall bottom [mm] | 4.1 | 2.8 | 3.8 | 3.8 | 4.2 |
| Vertical displ. wall bottom [mm] | 13.8 | 13.1 | 12.3 | 11.6 | 11.3 |
| Extreme bending moment [kNm/m] | 72.6 | 60.5 | 60.9 | 60.6 | 60.0 |
| Anchor forces [kN/m] | 201 | 195 | 196 | 195 | 194 |

Table 19: Stage No. 6: installation of 2nd row of anchors, hinge-end point at wall bottom

| | Plaxis | G5 S**3** | G5 S**4** | G5 S**5.1** | G5 S**5.2** |
|---|---|---|---|---|---|
| Heave of the pit bottom [mm] | 64.1 | 52.1 | 65.0 | 61.5 | 62.0 |
| Horizontal displ. wall top [mm] | 29.0 | 20.2 | 21.2 | 20.2 | 20.1 |
| Horizontal displ. wall bottom [mm] | 4.1 | 2.7 | 3.6 | 3.6 | 3.9 |
| Vertical displ. wall bottom [mm] | 14.6 | 13.6 | 12.9 | 12.2 | 11.9 |
| Extreme bending moment [kNm/m] | 37.6 | 47.8 | 48.8 | 48.3 | 50.0 |
| Anchor forces [kN/m] | 178/150 | 177/150 | 176/150 | 176/150 | 176/150 |

Table 20: Stage No. 7: excavation up to depth of 8 m, hinge-end point at wall bottom

| | Plaxis | G5 S**3** | G5 S**4** | G5 S**5.1** | G5 S**5.2** |
|---|---|---|---|---|---|
| Heave of the pit bottom [mm] | 68.3 | 55.7 | 69.6 | 66.2 | 67.3 |
| Horizontal displ. wall top [mm] | 62.9 | 36.5 | 39.2 | 37.2 | 37.4 |
| Horizontal displ. wall bottom [mm] | 8.7 | 5.1 | 6.5 | 6.4 | 6.9 |
| Vertical displ. wall bottom [mm] | 29.7 | 23.0 | 22.8 | 21.7 | 21.5 |
| Extreme bending moment [kNm/m] | 198.3 | 150.5 | 150.9 | 150.1 | 150.1 |
| Anchor forces [kN/m] | 251/186 | 222/192 | 222/193 | 220/191 | 220/191 |

Stage No. 3: excavation up to depth of 3.5 m

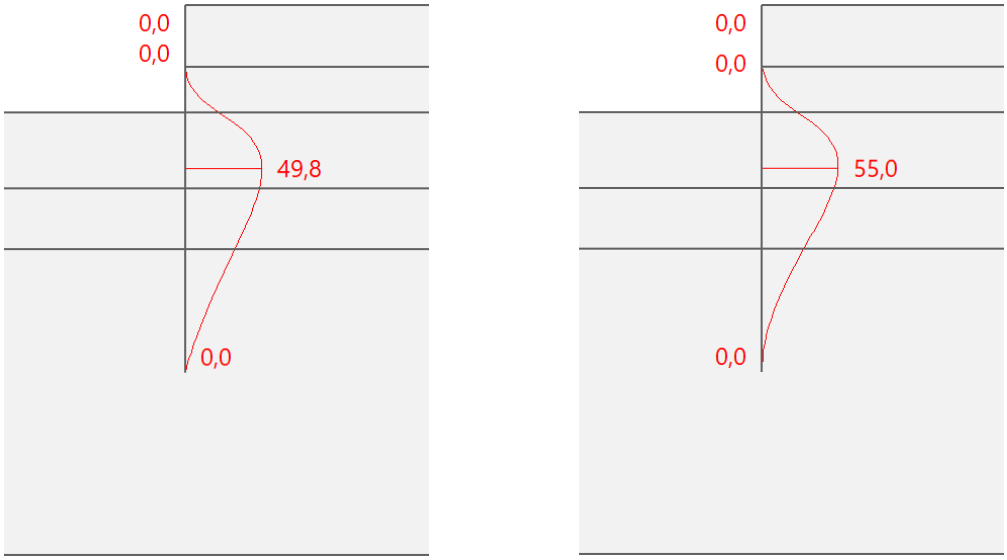


Stage No. 6: installation of 2nd row of anchors

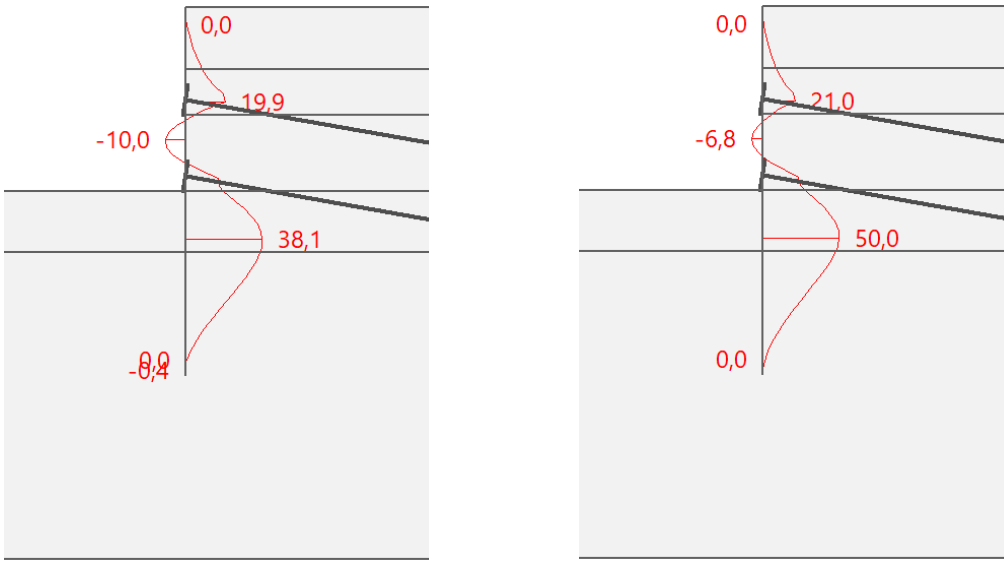


Stage No. 7: excavation up to depth of 8 m

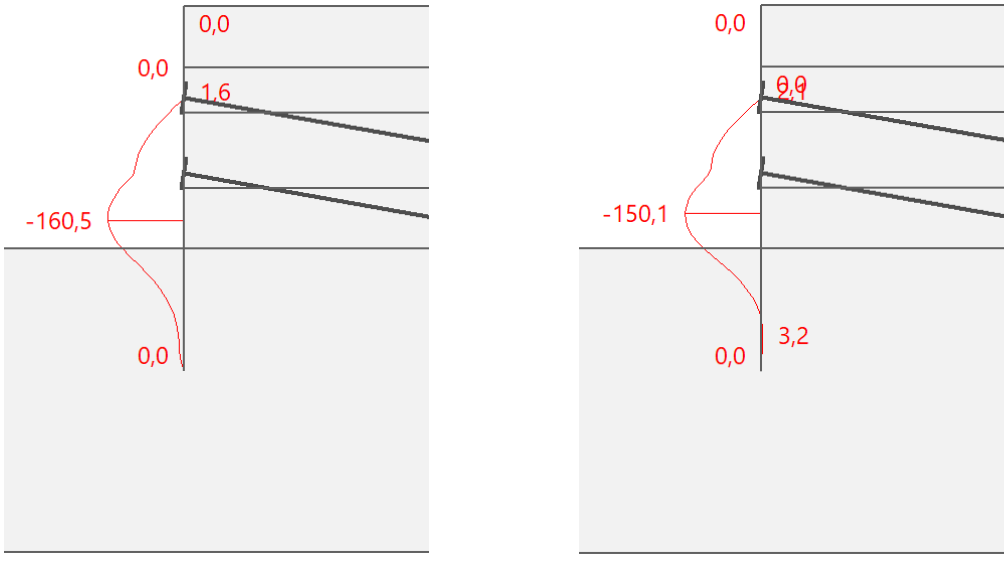


Figure 28: Comparison of **bending moments**: GEO5 FEM soil No. **5.2** foot (left), hinge (right)

It is evident from Tables 16 - 20 that vertical displacements of wall bottom predicted by GEO5 FEM are now comparable with those provided by Plaxis. We also observe a slight increase of horizontal displacements. But from an engineering point of view this change is essentially negligible. This applies also to the change in anchor forces when comparing their values found for the foot-end and hinge-end points of the wall. However, a noticeable difference is seen in the evolution of bending moments associated particularly with the prestressing step. The increase in the maximum bending moment for the case of hinge-end point is clearly evident for the 2nd row of anchors, see Fig. 28. The prestressing step is perhaps also the source of a difference between Plaxis and GEO5 FEM predictions most probably associated with the issue of elastic stiffness calculation.

In overall, this example demonstrates that a relatively simple modification to a computational model may result in appreciated changes in the predicted values of some of the parameters as is the case of internal forces in the present study. From the modeling point of view, the hinge-end point of a sheeting wall is generally not recommended.

# 6 Conclusion

From the simulation of two specific tasks, namely the strip footing and anchored sheeting wall, we observed that:

- There is no striking difference in the predictions provided by GEO5 FEM for individual sets of data. Thus if no information about the model parameters of a given soil is provided it is recommended to adopt the calibration software ExCalibre to deliver the desired parameters. This software is available free of charge in [1].
- In terms of displacements a somewhat stiffer response was delivered by GEO5 FEM in comparison to Plaxis for both selected examples. But from engineering point of view, the compared predictions are still reasonably close.
- When addressing the bending moments it is fair to mention that other issues, apart from HSM, such as the way of introducing anchors or the formulation of interface model, may play an important role, although this has not been observed for the Mohr-Coulomb model. The end-to-end point anchors were already mentioned. As for the interface elements, the reader is referred to theoretical manuals [2, 3] for more details.
- What has in general been observed is a relatively strong influence of the stiffness formulation, recall Eqs. (1) and (2), in the prediction of the displacement field and potentially other fields as well. Albeit different formulation, both softwares deliver the same response in pure compression where the influence of stiffness formulation is excluded. Thus the differences in the formulation of the preconsolidation pressure evolution play a minor role.

# References


[1] ExCalibre team. https://soilmodels.com/excalibre/.

[2] Fine ltd. *Theoretical manual*. http://www.fine.cz/.

[3] PLAXIS. *Theoretical manual*. https://www.bentley.com/software/plaxis-2d/.